This manuscript was accepted by Rev. Sci.Instrum. Click here to see the version of record.

Spatially resolved solid-phase temperature characterization in a sillimanite tube furnace using a broadband two-color ratio pyrometry

Sneh Deep[a)], Gopalan Jagadeesh
Department of Aerospace Engineering, Indian Institute of Science, Bangalore-560012, India

Tube furnaces are heating devices used for the synthesis of inorganic and organic compounds. It is essential to predict the spatially-resolved temperature of solid substances placed inside tube furnaces in contact with its walls, for a fixed steady temperature of the furnace walls. This enables efficient study of transport phenomena and control of the fabrication process in the furnace. In this work, the two-color ratio pyrometry (TCRP) using a digital single lens reflex camera has been used for the temperature characterization of a stainless steel (SS) metal sheet placed at the center of a 1000 mm long tube furnace. Temperature was measured for furnace walls set between 1000 K- 1426 K. The TCRP technique accounted for intensity from the heated target over the broadband visible region. The camera was calibrated and tested for signal linearity in its color channels, for a fixed source illumination. The technique yields a mean sheet temperature of 979.5 K ± ~24% (attributed to camera noise and uncertainties in gray level intensity, calibration lamp output; and monochromator and photodetector efficiency) and 1391 K ± 6.7% for a furnace wall temperature of 1000 K and 1426 K respectively. Experiments showed that the effect of distance between the target and the camera on temperature measurement was negligible. Emission spectroscopy in the Vis-NIR region (650-1100 nm) was also performed to predict sheet temperature. It yields results within 4.5% of TCRP at low furnace temperature but deviates by about 8.6% for temperature above 1150 K, most likely due to experimental errors in spectroscopy. Analytical heat balance on the sheet, IR imaging and numerical simulations yield temperatures within 5% of TCRP. This work shows that the TCRP technique can be used for spatially resolved temperature measurements of metals in tube furnaces and can readily be extended to ceramics or other class of solid materials whose emissivity can be shown to be invariant with wavelength in the visible region.

1. Introduction

Tube furnaces are heating devices based on the heating effect of electric current, used mainly for the syntheses of compounds, both organic and inorganic.[1-4] Many fabrications involve placing the reactants on the heated wall (working tube) of the furnace under a controlled environment. Che et al. deposited a thin film of Ni catalyst in the pores of an alumina template membrane by placing the latter in a sealed tube furnace at a pre-adjusted temperature.[1] Hu et al. fabricated tubular structures of SnO2 by oxidation of elemental tin placed in a horizontal tube furnace in the presence of a catalyst.[2] Furnace temperature was increased to a high value, maintained constant for about 30 min and then allowed to cool to room temperature to yield the required compound. Wu et al. synthesized faceted hexagonal aluminum nitride (h-AlN) nanotubes by simply nitriding aluminum powder and keeping the mixture in a tubular furnace.[3] Here too, the furnace was heated to a predetermined temperature critical to the synthesis process in an inert argon atmosphere. Liu et al. performed solid-phase reactions under administered temperature and time in a tube furnace for synthesizing organic 1D nanomaterials.[4] As clearly evident from the above text, temperature is one of the most important factors dominating the performance of ceramic tube furnaces. It is of utmost importance to know the spatial distribution of temperature of the solid-state substance placed in contact with the walls of the furnace, for a given final temperature of the heating coils in the furnace, often set manually and displayed on a screen. This not only helps in the proper control of the chemical synthesis process, but also enables intelligent study of mass transport and chemical processes occurring after attainment of an equilibrium temperature at the end of the heating cycle.[5]

For reactants that form gaseous molecules, the rate of atomization depends on the gas phase temperature in tube furnaces. Atomic absorption spectroscopy is commonly performed to study the characteristics of the synthesized products and the bulk crystals, with gas temperature playing a major role in the formation and detection of atoms.[6] It is for this reason that temperature evolution of the gas phase in tube furnaces has been studied extensively in open literature. Sperling et al. used coherent anti-Stokes Raman scattering (CARS) to study gas phase temperature distribution in a transversely heated graphite tube atomizer[6] and demonstrated its superiority over longitudinally heated atomizer for attaining isothermal wall conditions. Welz et al. also reported the longitudinal gas phase temperature difference between the tube center and its ends in a Massmann-type graphite tube furnace.[7] Frech and Baxter carried out measurements of characteristic masses of various elements using an isothermal atomizer and compared them with theoretical data to determine the effect of temperature on atomization efficiency.[8] For effective atomization conditions,

[a)]Corresponding author
Electronic mail: snehdeep@iisc.ac.in

a Massmann-type furnace was used. L'vov et al were the first to report gas phase temperatures in a graphite furnace using a "two-line method".[9] Although sufficient gas phase measurements exist, solid phase temperature characterization of the analyte in a tube furnace has hardly been reported by researchers. For reasons mentioned in the previous paragraph, knowledge of the latter is as important as that of the gas phase temperature and hence deserves a study. This will also facilitate characterization of the furnace from time to time, thereby establishing a relation between the displayed temperature and the solid substance temperature.

Several temperature measurement techniques have been developed and improved over time for temperature measurement in both gaseous and solid media.[10-14] Thermocouples and gas-sampling probes are examples of the former type, i.e., instruments for measurement of gas temperatures. Although easy to manufacture and use, they have several disadvantages such as poor response time, prone to damage in severe flow environment and single point measurement. Optical technique such as planar laser-induced fluorescence (PLIF) is also limited only to gaseous media and requires expensive equipment. Two common temperature measurement techniques in tube furnaces for gaseous phase are coherent anti-Stokes Raman scattering spectroscopy (CARS)[6,7] and a "two-line" method based on atomic absorption measurements at two lines of an element.[9,15] CARS offers several disadvantages- generation of background radiation, expensive hardware, and test sample susceptible to damage with high-power lasers to name a few.[16] Two-line method, on the other hand, is a line-of-sight (which is a heterogeneous temperature zone) integrated technique and may often yield imprecise results owing to ratioing of small absorbance with high signal-to-noise (SNR) ratio.

A well-known technique for measuring temperature of solids is infrared radiometry using infrared (IR) cameras and based on the relation between radiant intensity of the source in the infrared regime and its temperature. Infrared radiometry however necessitates knowledge of the emissivity (ε) of the source as a prerequisite for accurate measurements. This is seldom a constant and difficult to determine in reacting media such as those in tube furnaces. Another technique for temperature measurement in solid phase is multi-wavelength pyrometry- which records radiant intensity from the source at two or more discrete wavelengths, computes a ratio between them and relates them to temperature via a suitable calibration of the pyrometer.[17-19] A minor, recent variant of this technique uses a commercial digital camera as a pyrometer.[20-22] The technique is relatively inexpensive, does not require the source emissivity to be known, and is non-intrusive to the source. Known as the two-color ratio pyrometry (TCRP), the usage of a camera introduces another advantage- spatially resolved temperature measurement. Different types of tube furnaces have slowly made their way into research laboratories across the world, viz., top-fired co-current tube furnace, vacuum furnace heated by radiant tube burners, graphite tube furnace, rotary furnace, Massmann-type furnace, multizone furnace, etc. They have been used for several types of fabrication purposes as stated above, including some smart gauge preparations such as that done recently, which involved synthesis of large carbon cluster layers (LCC) by a single-step pyrolysis technique for development of thermally stable heat flux gauges.[23] This and many other analyte preparations sometimes require careful temperature measurement at several points on the surface of the analyte for gradient measurement which in turn enables knowledge of heat conduction in the analyte. Thermocouple measurements on smart gauges are few in literature, and those existing measure temperatures at a single point. Hence, the requirement of a spatially-resolved temperature measurement technique cannot be overemphasized.

In this work, we use the TCRP technique with a Digital Single Lens Reflex (DSLR) camera as the pyrometer to measure temperature of a thin, flat stainless steel (SS) plate placed in contact with the wall of a tube furnace. To the best of our knowledge, for the first time temperature has been measured for a representative solid state substance in a tube furnace. Steady state, spatially resolved 2D temperature measurements of the solid plate are carried out for different set temperatures of the working tube of the furnace, ranging from 1000 K-1426 K. This permits ascertaining the difference between the actual solid temperature and the temperature on the furnace display. The TCRP technique was developed independently in the laboratory by the authors. The camera was pre-calibrated with a calibration light source before being used as a pyrometer. A separate experiment was also performed to test the linearity of the intensity signal with exposure duration, for a fixed illumination. A fact that forms the backbone of the technique is that the radiating solid behaves as a gray body in the wavelength range of interest (visible, 400-700 nm).[24] A gray source is one whose emissivity remains constant with wavelength. Raj and Prabhu[18] used a CCD camera working in the visible region to measure temperature and emissivity of stainless steel using the colorimetric ratio method. By dividing intensity obtained in the green channel by the black body intensity and comparing the ratio with that in the red channel, they concluded that the gray body assumption is valid for stainless steel in the visible region. Their experiments were also conducted for plate temperatures close to 1000 K. Zander[21] used TCRP to measure the surface temperature of a heated C-C ceramic material assuming gray body radiation and showed the results to agree reasonably well with those obtained from a pyrometer measurement. This helped conclude that the particular ceramic material behaves as a gray body in the visible regime. The TCRP technique using a DSLR camera may be extended to other metals and ceramics if they can be shown to behave as a gray body in the visible region through conclusive measurements.

This manuscript was accepted by Rev. Sci.Instrum. Click here to see the version of record.

Next, the results were compared with emission spectroscopy performed in the tube furnace. An analytical heat balance was also performed on the SS sheet for various furnace wall temperatures to obtain the steady state temperature of the plate. To complement experimental results, 2D numerical simulations were performed in Ansys Fluent. Calculations are also influenced by a large number of uncertainties creeping up from the measurement principle, test conditions and the experimental set up. An analysis of the measurement uncertainties is also provided. All the experiments were conducted at the Laboratory for Hypersonic and Shock Wave Research (LHSR), Indian Institute of Science (IISc). Details of the work outlined in this paragraph are furnished in devoted sections and sub-sections that follow, together with the results and discussion.

2. Experimentation

2.1. Test Facility and Test Sample

The experiments were performed in an inhouse Lenton horizontal tube furnace[25], LTF 12/100/940, having a maximum operating temperature of 1473 K and a maximum power of 4000 W. The working tube has an inside diameter of 100 mm and a total length of 1000 mm, of which only 940 mm constitutes the heated length. The ends of the tube are open to the atmosphere, with 30 mm on each end unheated, as specified by the manufacturer. A wire element with high resistance is wound around the work tube and heats it up when power is supplied. Electronic controls are provided at the base of the furnace. A photograph of the furnace has been shown in Fig. 1, for reference. Also shown in the figure is a photograph from the front, showing the white colored working tube, inside which samples are placed for synthesis. The working tube is fabricated from an aluminosilicate mineral called sillimanite (Al_2SiO_5).

A stainless steel rectangular metal sheet was used as the test sample. It has a thickness of 0.32 mm, a height of 69.85 mm and a width of 50.8 mm. Since the TCRP technique is independent of the emissivity of the heated sample, the experiments may be repeated with any other class of material like ceramics to determine its temperature.

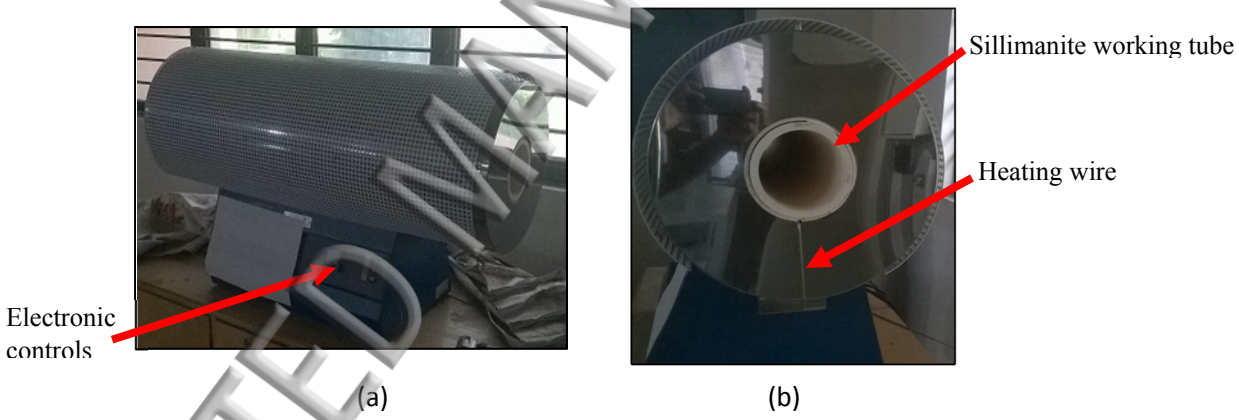

Fig. 1. (a) Photograph of the Lenton horizontal tube furnace with the electronic controls marked; (b) A front photograph of the same furnace, showing the hollow working tube inside which samples are kept.

2.2. Two-color ratio pyrometry (TCRP) equipment and physical model

A Canon EOS 750D DSLR camera, provided with a lens system of 18-55 mm focal length was used as a pyrometer to acquire the radiant intensity emitted by the heated metal piece in the form of unprocessed grayscale 'RAW' images. The camera has a CMOS sensor, sensitive in the visible region (in conjunction with an IR filter) and possesses a high spatial resolution of 24 megapixels. On top of the sensor lies a color filter array (CFA) or a 'mosaic' sensor- a collection of filters in three different color channels (red, green and blue)-which facilitates production of color images from the grayscale image by an interpolation algorithm known as demosaicing. The final full-scale color image provides RGB values at each pixel. Also, since the camera sensor has a large bit-depth of 14 in each color channel, it enables high precision in expressing the intensity magnitude.

Any real body with an emissivity ε and at an equilibrium temperature T emits energy in the form of radiation spanning the entire wavelength range of the electromagnetic spectrum. The spectral radiance per unit area of the body, per unit solid angle, per unit wavelength λ, denoted as L_λ, is accurately described by the Planck's Law proposed by Max Planck in 1900. It is given by Eq. (1) as

$$L_\lambda(\lambda,T) = \varepsilon(\lambda,T)\frac{C_1}{\lambda^5}\frac{1}{\exp(C_2/\lambda T)-1} \quad (1)$$

where $C_1 = 3.74 \times 10^{-16}$ W/m^2 and $C_2 = 1.44 \times 10^{-2}$ mK are constants based on the Planck's constant h, the speed of light c, and the Boltzmann constant k. ε for real bodies is always less than 1.

The equation relating the spectral radiance to the camera's sensor response R is given in the general form by Eq. (2)[26]

$$R_i = f_i \Delta A_d \varphi_i \Delta\omega_d \frac{\Delta t}{F^2}\int_{\lambda_1}^{\lambda_2} \chi_i(\lambda) L_\lambda d\lambda + n_i, \qquad i = R,G,B \quad (2)$$

where R_i is the pixel value in channel i in arbitrary units obtained after the optical system performs an A/D conversion on the original input, L_λ is the spectral radiance given by Eq. (1), $\chi_i(\lambda)$ is the spectral sensitivity of the optical system including the color filter array in channel i, ΔA_d is the pixel area, $\Delta\omega_d$ is the solid angle subtended by the pixel, φ_i is the gain of the electronics in the i^{th} channel, Δt is the exposure duration, F is the lens aperture, n_i is the dark signal in the i^{th} channel, and f_i is the intensity response function in channel i. λ_1 and λ_2 are the wavelength limits beyond which the sensor output is almost zero (in our case, the limits are 400 nm and 700 nm respectively).

In order to determine the intensity response function f_i of the Canon EOS 750D color camera, the following methodology was adopted. A dark signal, n_i was first obtained in each color channel by acquiring an image after closing the camera lens. It was then subtracted from the sensor response in the respective channel. Defining illumination as in Eq. (3)

$$I_i = \frac{\Delta A_d \varphi_i \Delta\omega_d}{F^2}\int_{\lambda_1}^{\lambda_2} \chi_i(\lambda) L_\lambda d\lambda \quad (3)$$

Therefore,
$$R_i - n_i = f_i I_i . \Delta t \quad (4)$$

Experiments were performed to determine the relationship between $(R_i - n_i)$ and (Δt) by acquiring irradiance images of a calibration lamp of fixed illumination at different camera exposures. Since the luminous intensity of the lamp was too high, neutral density filters (NDFs) effective in the entire visible region were used to diminish the intensity, so as not to saturate the pixels. NDFs ideally, by definition, possess constant spectral transmittance in the visible region and therefore their transmittance has not been separately considered in this work. All post-processing options on the camera were disabled and it was made to acquire uncompressed, raw images. The aperture was fixed at F5.6 for linearity-test experiments and the sensor sensitivity (ISO) level was maintained at the lowest value of 100 to prevent a 'grainy' image. The raw images were later processed in MATLAB with just the optimum steps so as not to adulterate the source intensity information. Images were acquired at shutter speeds ranging from 1/4000 sec to 1/5 sec for a fixed lamp illumination I. Fig. 2 is an illustration of the relationship between $(R_i - n_i)$ and the exposure normalized with the highest value of 1/5 sec and ranging between 0-1. The simple linear regression model was used to obtain the parameter estimators after minimizing the sum of squared residuals by the method of least squares. Once the parameters are known, the best fit straight line is obtained for the scattered data in each colour channel and have been shown. The equation of the best fit line is also mentioned in Fig. 2. The coefficient of determination (R^2), indicating the quality of the linear regression model was calculated to be 0.9998, 0.9988 and 0.9994 for the R, G and B channels respectively. These value are very close to 1, indicating an excellent linear relationship between $(R_i - n_i)$ and (Δt) for a fixed illumination I_i. If the proportionality coefficient be taken as c_i in color channel i, Eq. (2) may be rewritten as

$$R_i - n_i = \Delta A_d \Delta\omega_d \frac{\Delta t}{F^2}\int_{\lambda_1}^{\lambda_2} \varphi_i c_i \chi_i(\lambda) L_\lambda d\lambda, \qquad i = R,G,B \quad (5)$$

Replacing $\varphi_i c_i \chi_i(\lambda)$ with an effective spectral responsivity $\zeta_i(\lambda)$ and using the expression for L_λ from Eq. (1), the final expression may be written as

$$R_i - n_i = \Delta A_d \Delta\omega_d \frac{\Delta t}{F^2}\int_{\lambda_1}^{\lambda_2} \zeta_i(\lambda).\varepsilon(\lambda,T)\frac{C_1}{\lambda^5}\frac{1}{\exp(C_2/\lambda T)-1} d\lambda, \qquad i = R,G,B \quad (6)$$

In addition to the linearity test just elucidated, in order to relate the noise corrected pixel output $(R_i - n_i)$ to the source temperature T, it is imperative to know the effective spectral responsivity $\zeta_i(\lambda)$ of the color channels, the emissivity of the source ε, and other constants appearing in Eq. (6) before the integral. A blackbody calibration of the camera performed on the basis of the above equation will clearly be inaccurate. This is because the constants depend on the exposure duration and the distance between the camera and the source, which cannot be guaranteed to be the same during the calibration and actual experimentation. Moreover, the emissivity varies significantly from one material to another and must be eliminated. TCRP overcomes this complication by taking a ratio of detector signals for two different channels i_1 and i_2 to yield Eq. (7)

$$\frac{(R_{i_1}-n_{i_1})}{(R_{i_2}-n_{i_2})}=\frac{\int_{\lambda_1}^{\lambda_2}\zeta_{i_1}(\lambda).\frac{C_1}{\lambda^5}\frac{1}{\exp(C_2/\lambda T)-1}d\lambda}{\int_{\lambda_1}^{\lambda_2}\zeta_{i_2}(\lambda).\frac{C_1}{\lambda^5}\frac{1}{\exp(C_2/\lambda T)-1}d\lambda} \quad (7)$$

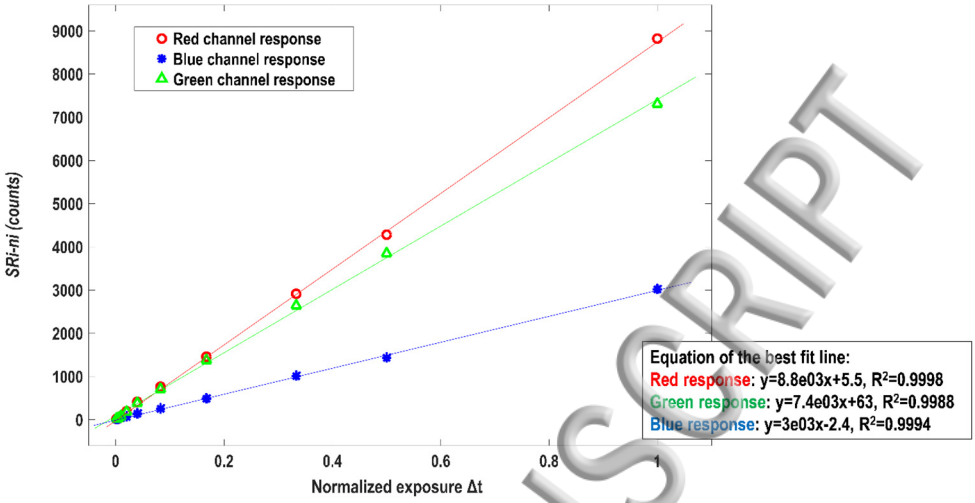

Fig. 2. EOS 750D camera linearity test in each color channel with respect to exposure for a fixed source illumination.

All the constants get cancelled in the ratio and need not be known explicitly. Also, with the gray body assumption mentioned in the introduction, the emissivity for the solid metal in our experiments vanishes. The ratio may be readily obtained for different temperatures by evaluating the integrals in Eq. (7) numerically (by discretization of the equation for sampled wavelengths) after determining the spectral responsivity $\zeta_i(\lambda)$ of the optical system in each channel. This is done by calibrating the DSLR camera against a source of known spectral radiance, the procedure for which is explained next. The transmissivity of the lens may also have an effect and has been included in the calibration procedure.

2.3. Canon EOS 750D Camera calibration- utilization of full visible spectrum

The optical set-up used in this work for camera characterization uses a calibration tungsten-halogen light source (lamp) with a known intensity vs. wavelength curve (provided by the manufacturer), a suitable hand-operated monochromator, the camera and a silicon-biased photodetector with known quantum efficiency. For technical specifications of the optical components, the reader is referred to the work of Deep et al.[27] Monochromatic light stimuli were presented to the Canon EOS 750D in steps of 10 nm in the visible region of 400-700 nm. Monochromatic stimulus was obtained by passing light from the calibration lamp through a monochromator, an optical device that splits incident radiation into its spectrum by dispersion. By manually operating a diffraction grating, a very narrow band of wavelengths centered at a specific wavelength can be obtained at the output slit. The calibration lamp was left switched on for about 10 minutes to obtain a stable output. All the images were obtained in the "RAW" format. After following a data-processing pipeline in MATLAB, the RGB values at sampled wavelengths were corrected for monochromator efficiency and then divided by the lamp's intensity at the respective wavelength independently to determine the spectral responsivity $\zeta_i(\lambda)$ in each channel. Next, the product of the responsivity and Planck's analytical spectral output for a temperature was computed at sampled wavelengths. This yields three simulated response curves, one for each color channel. The total area under each curve was calculated and ratio obtained for each combination of color channel. By repeating the process for many temperatures, a look-up table (calibration curve) between source temperature and pixel value ratio was obtained. The calibration curve for each combination of color channel has been shown in Fig. 3. A noteworthy point is that the calibration has been limited to the visible wavelength range of 400-700 nm. This is because the DSLR camera is internally provided with an infrared cut filter just before the CFA, which prevents any light in the IR region from falling on the sensor. Due to the IR filter, the effect of radiation above 700 nm will be negligible.

The monochromator efficiency was determined by replacing the camera with the photodetector of known spectral response. Fig. 4 illustrates the simulated response curves in each of the RGB color channels for a temperature of 2000 K, along with the Planck's spectral radiance. The set-up for determination of monochromator efficiency is also shown.

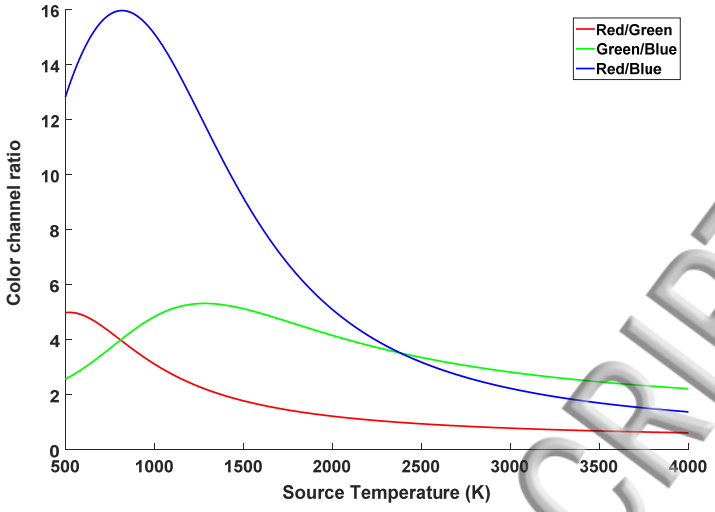

Fig. 3. Source temperature (K) vs. Color channel ratio for various combination of color channels.

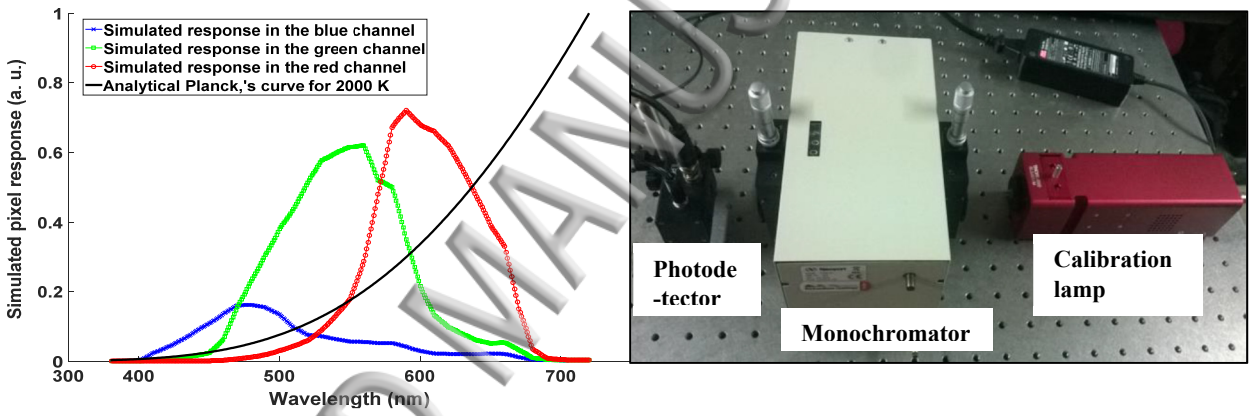

(a) (b)

Fig. 4. (a) Simulated pixel response from the Canon EOS 750D camera for a source temperature of 2000 K; (b) Set-up for monochromator efficiency determination. For camera calibration, the photodetector was replaced by the camera.

2.4. Data Processing

The Canon EOS 750D has a provision for acquiring images in the raw format and the compressed, internally processed format simultaneously. Therefore, we procured images in the raw *.cr2 format for TCRP and in the processed *.jpg format for presentation purposes. The *.cr2 image was converted into a different format, *.dng using Adobe's proprietary open-source software called Adobe DNG Converter. This file is easily read into the MATLAB programming language. A dark image procured at the same exposure was subtracted from the raw image to get a thermal noise-free image. The corrected image contains intensity information of any one of the three color channels (R, G or B) in each pixel, depending on its position with respect to the CFA. In that sense, it is a gray-scale image. It was converted into a full color image, with a bit-depth of 14 in each channel, by a demosaicing technique[28]- one that interpolates the missing color information for each pixel from its neighbors. The resulting color image was then cropped to the region of interest to save computational time and color value ratio was obtained on a pixel-by-pixel basis and mapped to the corresponding temperature based on the look-up table generated from calibration. This yields the final 2D temperature field.

2.5 Experimental configuration

The stainless steel (SS) sample, described earlier, was placed at the center of the heated walls of the ceramic working tube. The working tube is open at both ends. The flat surface of the sample faces the camera directly, through one of the open ends, as illustrated in Fig. 5. The furnace is connected to a power supply, which heats up the walls of the ceramic tube as per the temperature setting done by the experimentalist. This in turn heats the metal, the radiant intensity from which is acquired by the camera. The effect of distance between the sample and the camera on the temperature is also studied, by varying the camera's distance from the furnace open end from 250 mm-1000 mm. For spectroscopic measurements, the camera was replaced by a spectrometer, equipped with an optical fiber. The optical fiber was used so that it could be held very close to the radiating metal, so as not to intercept any radiation from the walls of the furnace.

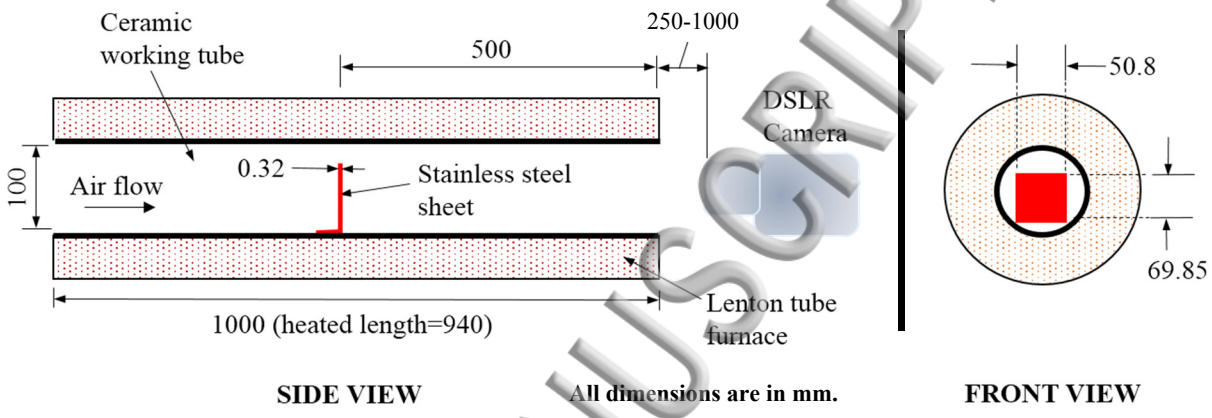

Fig. 5. A schematic of the experimental configuration showing the arrangement of the test sample, the tube furnace and the camera.

2.6. Numerical model

The experimental temperature results were complemented with numerical simulations performed in Ansys Fluent. 2D, planar geometry was generated to save computational time and the flow field was discretized with about 176,000 elements. The working tube was modeled, with the stainless-steel plate modeled at the geometric center. The governing conservation equations were discretized using the cell centered finite volume approach. A density-based, steady state solver was used as the temperature after attainment of steady state conditions on the metal plate were of interest. Calculations based on non-dimensional numbers showed that free convection dominates over forced convection and that the free convection boundary layer was laminar. Hence a laminar viscosity model was specified for the computations. The Surface-to-Surface (S2S) radiation model was chosen to account for radiation between the heated walls of the working tube and the metal surface. Air was taken as an ideal, incompressible gas, with constant values for isobaric specific heat (C_p), thermal conductivity (k) and viscosity (μ).

Suitable boundary conditions (BCs) were allocated to the flow domain, as illustrated in Fig. 6. Both inlet and outlet were maintained at a temperature of 300 K. A velocity-inlet BC was used at the inlet, with an air velocity of 0 m/sec as only natural convection exists during experimentation. A pressure-outlet BC was used at the outlet with normal atmospheric pressure specified. An isothermal, no-slip boundary condition was specified at the furnace walls, with an internal emissivity of 0.3 for sillimanite. The temperature of the wall was specified values ranging from 1000 K-1426 K and simulations were run for each temperature separately. The metal sample surface was also specified as a wall with mixed thermal BCs, which allows specifying inputs for both convective and radiative heating. The heat transfer coefficient (h) for convective heat flux was calculated analytically by using empirical relations for the Nusselt number and Prandtl number based on measured and known quantities. The value thus obtained was 10.6 W/m^{2}K. For radiative heat flux, the free stream temperature was fixed at 300 K and the emissivity was specified as 0.73 for steel. Since air is composed of nonpolar gases O_2 and N_2 which are essentially transparent to incident thermal radiation,[29] its temperature is expected to not rise too much from the initial room temperature of 300 K. As for the convective heat flux also, the free stream temperature was assumed to be 300 K. Since the actual temperature of air was unknown, 300 K was used with the intention of allowing maximum convective heat loss from the plate to the air. The simulation was run until all the residuals (continuity, x-velocity, y-velocity and energy) fell to at least 1×10^{-06}.

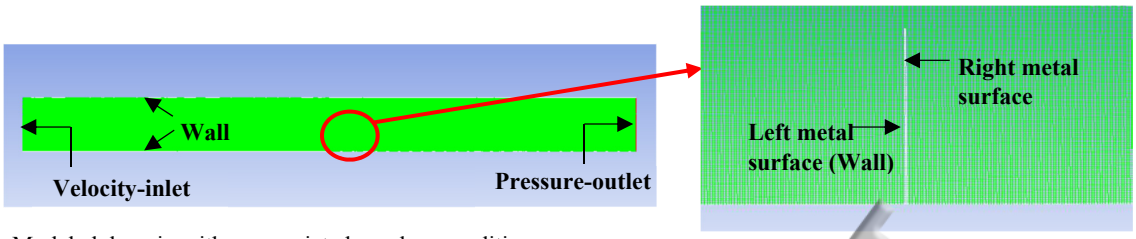

Fig. 6. Modeled domain with appropriate boundary conditions.

3. Results and Discussion

3.1. Images of the heated SS plate in the tube furnace and TCRP to determine spatially resolved temperature

The tube furnace was heated to temperatures ranging from 1000 K-1426 K, in multiples of 50 K, except for the last value. Separate experiments were performed for each temperature. For each experiment, as the working tube reached the set temperature (indicated on a screen), approximately 10 seconds were provided for the heat transfer process between the participating media to reach an equilibrium state, which was also obtained analytically and has been discussed briefly in Section 3.2. Thereafter, 50 continuous images of the heated metal plate were acquired by the camera. The lens aperture f-stop can be set between F5.6-F32. It was fixed at F10 for all the experiments in the tube furnace. The ISO was maintained at the lowest possible value of 100. The exposure was fixed so as not to saturate the pixels and depended on the temperature of the working tube, with higher temperatures requiring a lower exposure duration. The lens focal length was maintained at 55 mm. For each furnace temperature, the distance of the camera was varied from 250 mm-1000 mm in multiples of 125 mm. This was done to see the effect of distance on the final temperature result from TCRP. An average intensity image was obtained from the 50 continuous images to account for any small variations of plate surface temperature after attainment of a steady magnitude. The 50 images were also separately analyzed to check the variation in mean surface temperature from one image to another. It was found that the mean temperatures were within ±12 K between images for a furnace wall temperature of 1426 K, further consolidating the fact that the metal temperature reached equilibrium. Fig. 7 depicts a photograph of the averaged image for a distance of 375 mm for a few selected furnace wall temperatures. The exposure duration is mentioned below each image.

A dark, baseline image was also acquired at the same exposure with the camera lens closed. This was then subtracted from each raw image to eliminate the thermal noise generated in the camera due to its compact body. The Canon camera's CFA possesses a Bayer 'RGGB' alignment pattern[30]. This information was used to perform demosaicing in MATLAB, to obtain RGB values at each pixel. The R/G ratio was procured at each pixel and mapped to a temperature based on the characterization curve shown in Fig. 3. For the R/G ratio, as evident from Fig. 3, the curve reaches a maxima of 5 at a temperature of about 500 K. This is the maximum R/G ratio obtainable from the Canon EOS 750D filter/sensor combination. The 2D temperature map corresponding to the images shown in Fig. 7 have been illustrated in Fig. 8. The temperature scale on the right of each map is chosen so as to show the values of interest in detail.

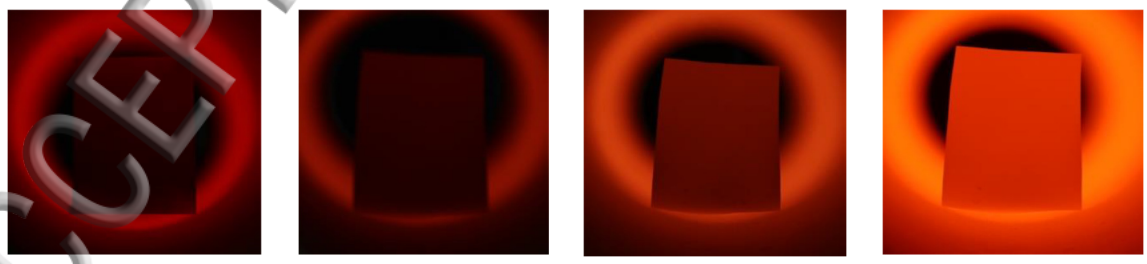

Fig. 7. Intensity-averaged photograph of the heated SS plate for selected furnace wall temperatures. The images are for a distance of 375 mm between the camera and the end of the furnace.

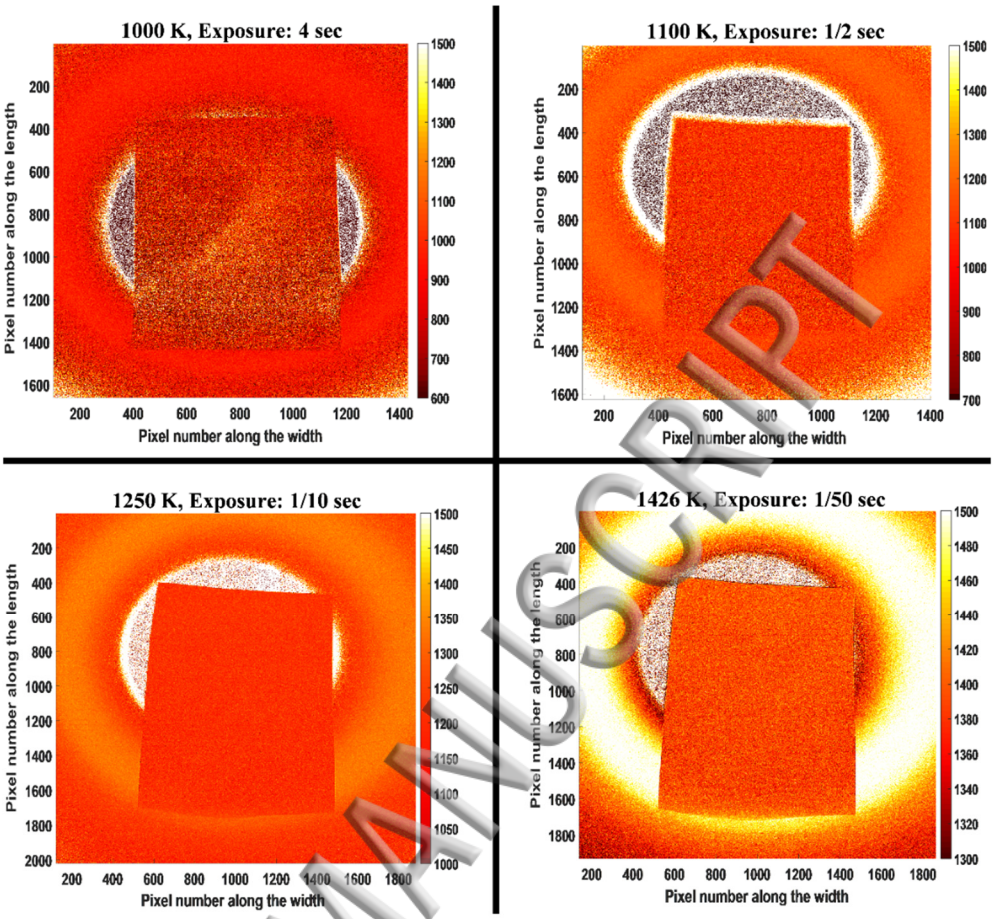

Fig. 8. 2D temperature map corresponding to the images of the heated plate in Fig. 7.

A mean temperature of the surface of the metal plate was calculated. It was inferred from Biot number calculations (shown later) that the lumped capacitance method is valid, according to which the temperature of the solid is uniform at any instant[29]. Hence no or very small temperature gradients were expected on the solid surface. For a furnace temperature of 1000 K, the mean sample temperature was 979.5 K ± 24% (due to camera noise and other uncertainties, elucidated in Section 4). For the highest furnace temperature of 1426 K, the mean surface temperature of the sheet was found to be 1391 K ± 6.7%. The uncertainty is found to be lower as the temperature of the SS sheet increases, due to reduction in noise. Higher temperatures in the circular region behind the metal plate in Fig. 8 is due to the fact that the region is dark and has extremely low SNR, leading to unrealistic temperature values. A filtered plot of temperature vs. position on the SS metal sheet, both in the horizontal and vertical direction is shown in Fig. 9 for a furnace wall temperature of 1426 K. The temperature along the line in the vertical direction oscillates about a mean value of 1393 K with a standard deviation of 26.6 K. The corresponding mean along the horizontal direction is 1395 K and a standard deviation of 25.5 K. The small values of standard deviation also indicate temperature invariance with position.

The G/B and R/B ratios, in addition to the R/G ratio, have also been used for temperature characterization of the SS sheet to compare the results. The calculations have been confined to the case when the furnace wall temperature is at 1426 K. Results can be extended to other furnace wall temperatures as well. The mean temperature on the SS sheet surface obtained from using the R/B and G/B ratio is about 1354.3 K and 1481 K respectively. These values are close to 1391 K obtained from the R/G ratio, thereby increasing confidence in the results. The corresponding figures of the temperature map obtained from the R/B and G/B ratio have been shown in Fig. 10. The noise in the temperature map from the G/B image is higher than its counterparts, perhaps due to multi-valued nature of the G/B vs. temperature curve. However, it does yield a mean temperature close to that from the other ratios. The agreement between these temperatures also suggests the accuracy of the gray body assumption for the SS sheet.

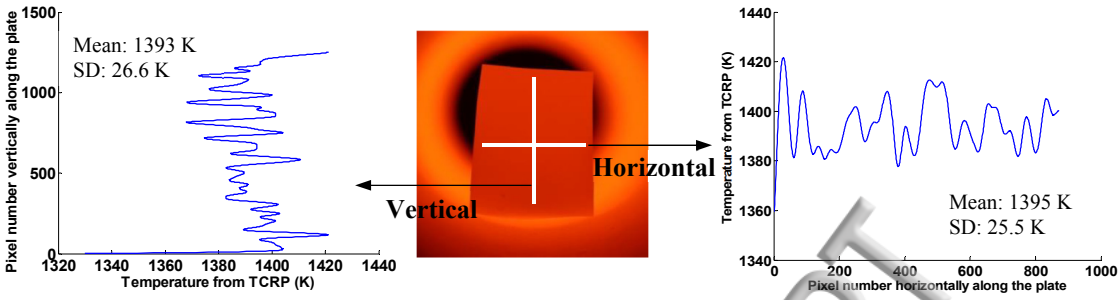

Fig. 9. Temperature variation along the vertical and the horizontal line for the heated SS plate when the furnace wall temperature is 1426 K.

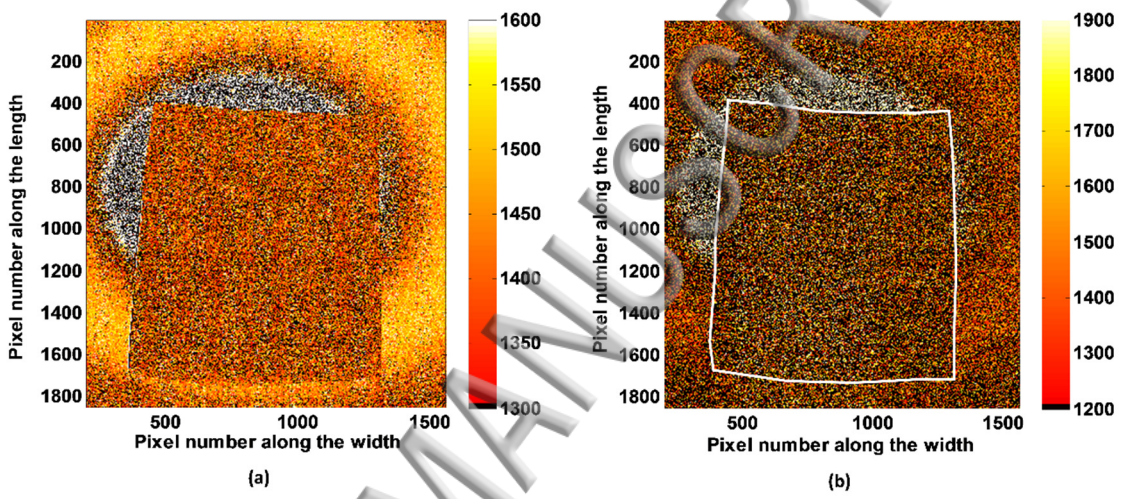

Fig. 10. 2D temperature map corresponding to (a) The R/B ratio; (b) The G/B ratio. The outline of the SS sheet has been shown in (b) based on an edge detection algorithm, as the image is quite noisy.

As mentioned earlier, the distance between the camera and the tube furnace was increased from 250 mm-1000 mm. The focal length was maintained constant at 55 mm. The variation in temperature of the SS sheet with distance was found to be negligible. Since TCRP is an intensity ratio-based technique, it may be inferred that as the distance increases, the intensity in both the red and green channels, while passing through the cold atmosphere, attenuates in a manner that the ratio remains essentially the same. Hence, similar temperature results are obtained.

3.2. Comparison with other techniques- Emission spectroscopy, analytical heat balance and numerical simulations

In the emission spectra of metals, there are wavelength regions where the radiance closely follows the blackbody spectrum. By comparing the spectra to a Planck spectrum as described in Eq. (1), the temperature of the subject may be determined. An Ocean Optics STS-NIR miniature spectrometer with photodetector arrays, operating in the visible-NIR (650-1100 nm) range was also used to acquire emission spectra from the heated SS sheet. The spectrometer offers a high SNR (>1500:1) and a high dynamic range (4600:1). It has a slit with adjustable width ranging from 10-200 µm, an optical resolution of 1.5 nm for a 25 µm slit, is thermally stable and provides easy connectivity and usage. The integration time ranges between 10 µs-10 sec. The spectrometer is provided with a grating of 600 lines/mm. Since a spatially invariant temperature was expected on the SS surface, a single integrated, continuous spectrum covering 1024 pixels on the metal surface was sufficient to ascertain it. The quality of the 'fit' or similarity between the experimental and the theoretical spectra is obtained by the classic method of least-squares. The technique minimizes the sum of the squared residuals, i.e., the difference between the recorded value and that obtained from the Planck model at discrete wavelengths.

The relative spectral sensitivity of the spectrometer was first determined using the same calibration lamp that was used to characterize the camera. A dark, background signal was first recorded and subtracted from the spectrum of the lamp as recorded by the spectrometer. The known intensity of the lamp (provided by the manufacturer) was divided by

the spectrum to get the calibration ratio. Since the calibration ratio showed an abrupt increase beyond 975 nm, the long-wavelength portion of the spectrum beyond 975 nm was discarded. The temperature was determined for a spectral region of 650 nm-975 nm. After the calibration, emission spectra were recorded for each of the 10 furnace wall temperatures (1000 K-1426 K) and the corresponding dark spectrum, obtained with the same integration time, was subtracted. A 1 m long optical fiber with lens arrangement was maneuvered very close to the SS sheet to concentrate light from the metal only, and no stray light from the furnace walls. In other words, the optical fiber was focused on the SS sheet and its field of view did not include the furnace interior walls. The spectrum was then corrected with the calibration ratio to get the actual intensity values in the NIR range. The final experimental spectrum was again normalized between 0-1. Likewise, the Planck's portion of the spectrum between 650 nm and 975 nm was also normalized for various temperatures. The least-squares method was then employed to determine the 'best fit' temperature for a given furnace temperature.

It is to be noted that since the knowledge of temperature necessitates recording only the relative radiation at different wavelengths, factors such as target dimensions and distance from it do not affect the results[31]. Fig. 11 shows the emission spectrum along with its best fit Planck's curve for wall temperatures of 1000 K and 1426 K. The R^2 values indicate the quality of fit. Planck curves have also been plotted for 850 K and 1050 K, two temperatures close to the value for which best fit was obtained (937 K). The Planck's curves for 850 K and 1050 K also agree to a good degree with the spectral signal, thus explaining the large uncertainty in temperature, as pointed out in the uncertainty analysis later. The temperature of the SS sheet thus determined from emission spectroscopy has been tabulated below, along with the coefficient of determination (R^2) indicating the quality of fit.

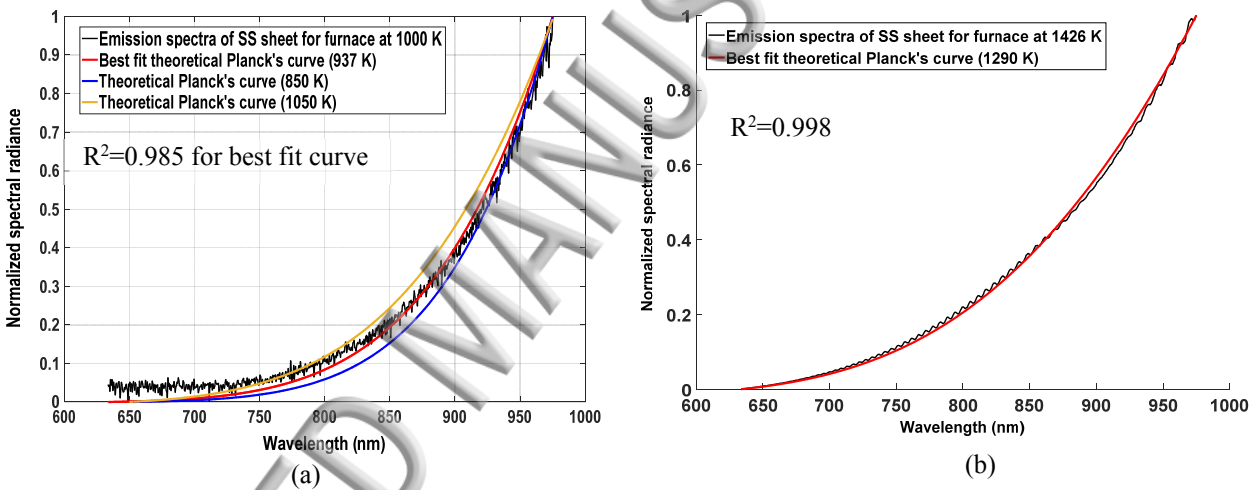

Fig. 11. Graph showing the quality of fit between the experimental spectrum and the theoretical spectrum from the Planck's law for (a) Furnace wall temperature at 1000 K, (b) Furnace wall temperature at 1426 K.

Table 1

SS sheet temperature from emission spectroscopy for different furnace wall temperatures.

Furnace wall temperature (K)	Temperature of SS sheet from emission spectroscopy (K)	R^2	Temperature of SS sheet from TCRP (K), for a distance of 375 mm between the camera and furnace
1000	937	0.985	979
1050	1014	0.958	1042
1100	1079	0.993	1084
1150	1130	0.994	1112
1200	1108	0.998	1160
1250	1148	0.998	1212
1300	1176	0.998	1288
1350	1223	0.998	1338
1400	1270	0.998	1387
1426	1290	0.998	1391

It is clear from Table 1 that emission spectroscopy yields result similar to those obtained from TCRP at low furnace temperatures up to 1150 K. The temperatures are within 4.5% of that obtained from TCRP. However, as the furnace

temperature is set to values beyond 1150 K, the spectroscopy results start differing from that of TCRP by a larger percentage, reaching as much as 8.6% for 1426 K. Since the form of the theoretical and experimental curves are compared to obtain the best fit, emissivity of the source need not be known for emission spectroscopy. In that sense, it is similar to TCRP except that there are hundreds of data points to ascertain the temperature, and not just a single ratio like in TCRP. Thus, emission spectroscopy is expected to be a lot more accurate than TCRP as it incorporates more data points. However, there is no spatial resolution as spectroscopy yields only one temperature for the entire plate surface. On the contrary, TCRP yields a temperature at closely spaced points all across the plate, which is what makes it so valuable.

A rough, analytical estimate of the SS sheet temperature for various furnace wall temperatures was also done. Fig. 12 shows a schematic of the sheet and the furnace wall, along with the various modes of heat transfer to the SS sheet. A simple heat balance has been performed on the SS sheet to determine its steady state temperature.

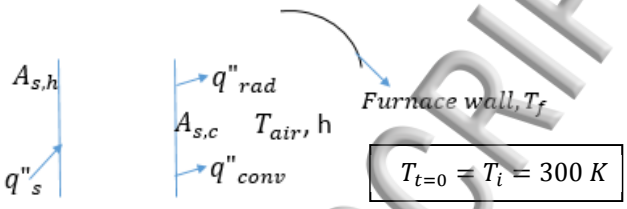

Fig. 12. Schematic of the SS sheet (blue) and the furnace wall (black), with various modes of heat transfer to the SS sheet shown.

$A_{s,h}$ is the cross-sectional area of the thin SS sheet, $A_{s,c}$ is the surface area of the SS sheet, q''_s is the conductive heat flux into the sheet, q''_{rad} is the net heat exchange between the sheet and the furnace walls due to radiation, q''_{conv} is the heat exchange between the sheet and the surrounding air due to convection, T_{air} is the temperature of the surrounding air, h is the heat transfer coefficient and T_f is the furnace wall temperature. Performing a heat balance of the SS sheet, one may write the general form of the heat balance equation as

$$q''_s A_{s,h} - \left[h(T - T_{air}) + \varepsilon\sigma\left(T^4 - T_f^4\right)\right]A_{s,c} = \rho V c \frac{dT}{dt} \tag{8}$$

$\rho = 7999.5$ kg/m^3 is the density of stainless steel, $c = 510$ J/(kg-ºC) is its specific heat, V is the volume of the sheet, $\varepsilon = 0.73$ is the emissivity of stainless steel, and $\sigma = 5.67 \times 10^{-8}$ Wm^{-2}K^{-4} is the Stefan-Boltzmann constant. The value of h was calculated to be 10.6 W/m^{2}K.

As stated earlier, a lumped capacitance method was chosen for the calculations, i.e., the temperature of the SS sheet was taken to be spatially invariant. The justification of this assumption is based on the Biot number, Bi, which in our case was 8.5×10^{-5}. Since it is less than 0.1, lumped capacitance approach is valid.[29] Table 2 lists the steady state temperature of the SS sheet obtained analytically for all the furnace wall temperatures. The term (dT/dt) was also equated to zero since a steady temperature of the metal sheet was required. T_f was equated to the corresponding furnace wall temperature for which the equation was solved. In order to determine the time required for the metal plate to reach an equilibrium temperature from the instant the furnace reaches its set temperature, the following procedure was adopted. The temperature of the furnace wall, starting at room temperature, was noted at regular intervals and was found to increase linearly with time. The corresponding linear expression was substituted for T_f in Eq. (8) and the equation was numerically solved marching forward in time, starting at the initial condition that the metal sheet temperature, $T_{t=0}$ =300 K. For a furnace wall temperature of 1426 K, calculations yielded a sheet temperature of 1400.4 K (just at the instant furnace reaches 1426 K). At this instant, (dT/dt) was calculated for T =1400.4 K and T_f =1426 K and was equal to 0.56. Also, for dT/dt =0, the steady state sheet temperature was 1401.05 K. Thus, the time required to attain steady state was about 2 sec. Similar calculations were done for all furnace wall temperatures, and the maximum time required for the metal sheet to attain steady state was about 4 seconds for the furnace wall at 1000 K. Therefore, while acquiring temperature equilibrium images of the metal sheet, a sufficient lead time of 10 sec was employed.

Table 2
SS sheet temperature from analytical calculations for different furnace wall temperatures.

Furnace wall temperature (K)	Temperature of SS sheet from analytical heat balance (K)
1000	955.04
1050	1008.34
1100	1061.32
1150	1114.02
1200	1166.47
1250	1218.7
1300	1270.7
1350	1322.54
1400	1374.2
1426	1401.05

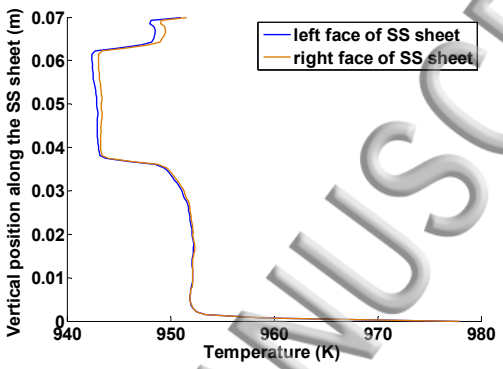

Fig. 13. Temperature distribution on the left and right surface of the SS sheet, for a furnace wall temperature of 1000 K.

Fig. 13 is a graphical representation of the temperature variation on the left and right faces of the metal plate, obtained from computations for a furnace wall temperature of 1000 K. The temperature along the length of the plate is nearly constant, the average on the left and right face of the SS sheet being 948 K and 949 K respectively. The mean right (or left) surface temperature of the metal plate for different furnace wall temperatures is reported below in Table 3.

Fig. 14 is a consolidated plot of the SS plate temperature obtained experimentally, analytically and numerically for different furnace wall temperatures. The figure suggests that the analytical solution and numerical calculations complement TCRP results very well. Emission spectroscopy follows TCRP up to 1150 K and then deviates. All the results show a linear increase in SS sheet temperature, as the furnace wall temperature is linearly increased. In principle, emission spectroscopy is expected to yield the most accurate results as the temperature is inferred from a large number of data points. The deviation of TCRP results from emission spectroscopy beyond 1150 K may be most likely due to experimental errors in the latter. As a final check of the accuracy of TCRP, a calibrated IR thermal imaging camera (single point measurement) was aimed at several locations on the heated SS sheet and the mean temperature was noted. The IR camera yielded a temperature of 940 K, 1340 K and 1353 K for a furnace wall temperature of 1000 K, 1400 K and 1426 K respectively. These values are within 4% of that of TCRP.

Table 3
2D SS sheet mean temperature from numerical simulations for different furnace wall temperatures.

Furnace wall temperature (K)	Mean temperature of right surface of SS sheet from numerical simulations (K)
1000	949.1
1050	999.77
1100	1048.7
1150	1100
1200	1151.2
1250	1200.4
1300	1253.5
1350	1301
1400	1347.45

1426	1377

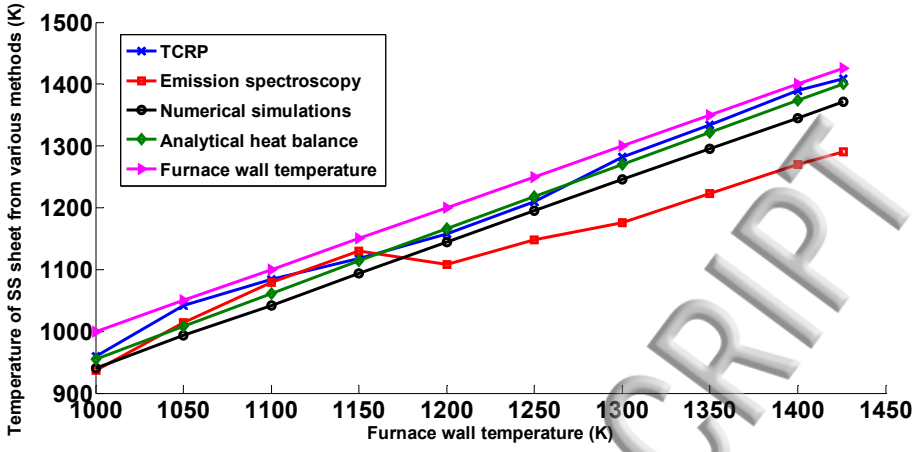

Fig. 14. Comparison of steady state temperature of the SS sheet from TCRP, emission spectroscopy, analytical heat balance and numerical simulations, for 10 different furnace wall temperatures between 1000 K and 1426 K.

4. Error and Uncertainty analysis

The experimental equipment used in this work, viz. the DSLR camera presents uncertainty in the results, mainly by way of noise. Several types of noise exist for color digital cameras; such as read noise which is negligible for commercial high-end cameras as used in our work, thermally generated dark noise which was minimized by subtracting a dark background image acquired by closing the lens cap, and fixed pattern noise which occurs due to variation in pixel sensitivity based on its position on the sensor and was addressed by repeating the camera calibration for different positions of the sensor intercepting light from the calibration lamp. The maximum difference in R/G ratio for two sensor positions for any temperature (1000 K-1500 K) in the calibration curve was a nominal 0.37% and hence has been neglected.

The variation in temperature on the SS plate as obtained from TCRP was also calculated. It varied from as high as ±22% on a mean plate temperature of 979.5 K, to 2% on a mean plate temperature of 1391 K. This may be attributed to noise. The variation therefore reduces to negligible levels as one uses TCRP for relatively higher temperature measurements. Apart from this, an analysis was performed to estimate the influence of radiation measurement uncertainties on the TCRP calculated temperature on the sheet. Since the camera produces discrete intensity counts, an average uncertainty of ±0.5% in grey level intensity was estimated while procuring the intensity count for each sampled wavelength (in the visible regime) and for each colour channel during the calibration process. Due to the uncertainty in camera intensity and therefore a modified intensity value, the color channel ratio vs temperature curve (also called calibration curve) would change, i.e., for a given ratio, the temperature would now be different than that previously. Also, while acquiring image of the source (SS sheet) during actual experimentation, the R and G intensities are considered to have ±0.5% uncertainty. Likewise, the modified R and G levels were used to evaluate a new R/G ratio and the temperature read off from the modified calibration curve. This was compared to the actual temperature and uncertainty was reported. The maximum absolute uncertainty in temperature thus obtained was 5.8% on the base temperature of 1000 K and 3.9% on the base temperature of 1426 K. These uncertainties, as evident, are those for the measurements on the SS plate surface. Regions that fall outside the plate surface emit negligible radiation and will possess unrealistic SNR. Hence, uncertainties in such regions have not been reported. Apart from this, the uncertainty in calibration lamp intensity is 0.05%, as provided by the manufacturer. For this uncertainty, the previous method was followed and the corresponding uncertainty in temperature thus obtained was 2.4% on the base temperature of 1000 K and 1.1% on the base temperature of 1426 K. The uncertainty in photodetector efficiency has not been provided by the manufacturer and hence a value of ±0.5% was assumed. This was first used to obtain the uncertainty creeping into the monochromator efficiency (as the latter is dependent on photodetector efficiency and was obtained during the determination of efficiency of the optical system) and then the obtained uncertainty in monochromator efficiency was used to determine the uncertainty in temperature. The exercise yielded a temperature uncertainty of 4.9% on the base temperature of 1000 K and 3.4% on the base temperature of 1426 K. Finally, an inherent uncertainty of 0.5% was assumed in the monochromator intensity output, which yielded a temperature uncertainty of 4.7% on the base

This manuscript was accepted by Rev. Sci.Instrum. Click here to see the version of record.

mperature of 1000 K and 3.7% on the base temperature of 1426 K. The uncertainty in emissivity and filter transmission would not affect the TCRP temperature as it is a ratio based technique and independent of both emissivity and transmissivity.

The cumulative uncertainty of a derived quantity is obtained as a root sum square of the corresponding uncertainties due to all quantities it is dependent upon. This is the standard method of computing uncertainties and was formulated by Moffat.[32] The cumulative uncertainty thus obtained from the individual uncertainties due to noise, camera intensity levels, the calibration lamp, the photodetector and the monochromator was ~24% for a base temperature of 1000 K and 6.7% for a base temperature of 1426 K.

Error in the presented analytical method of temperature estimation is also analyzed here. Simplification of Eq. (8), after assumption of negligible conduction and attainment of steady state gives Eq. (10)

$$-\left[h(T - T_{air}) + \varepsilon\sigma\left(T^4 - T_f^4\right)\right]A_{s,c} = 0 \tag{10}$$

In order to ascertain the influence of varying furnace wall temperature, surrounding air temperature, emissivity of the metal sheet, and heat transfer coefficient on the temperature of the SS sheet, a total differential of the above equation was taken and is given by Eq. (11)

$$dT = \frac{4\sigma\varepsilon T_f^3\, dT_f + h\, dT_{air} + \sigma\left(T_f^4 - T^4\right)d\varepsilon - (T - T_{air})\, dh}{h + 4\sigma\varepsilon T^3} \tag{11}$$

dT_f is the uncertainty in the furnace wall temperature available from the manufacturer of the furnace, dT_{air} is the uncertainty in the surrounding air temperature, dh is the uncertainty in heat transfer coefficient as it depends on several factors such as air velocity, sheet geometry, temperature, etc.; and finally $d\varepsilon$ is the uncertainty in the emissivity of the metal which may depend on temperature and wavelength. It is difficult to know the uncertainty value in each of the quantities. Therefore, a maximum uncertainty of ±10% is estimated in the values of T_f, T_{air}, ε and h. The uncertainty in metal plate temperature due to this range of uncertainties in the quantities on the right hand side of Eq. (11) were computed. A maximum uncertainty of +107.8 K (+11%) was obtained for an SS sheet mean temperature of 979.5 K when the furnace wall temperature was 1000 K. The corresponding uncertainty for a furnace wall temperature of 1426 K was +156.8 K (+11.2%) for the mean sheet temperature of 1391 K.

5. Conclusion

The aim of this work was to characterize the temperature of solid phase substances placed in the heated working tube of furnaces for their synthesis. Knowing the temperature of such substances for a given fixed temperature of the heating coils of the tube furnace enables appropriate control of the fabrication process and study of various transport phenomena during synthesis, as temperature is one of the most crucial parameters governing the entire process. A stainless steel (SS) metal sheet (69.85 mm × 50.8 mm × 0.32 mm) was used as the representative solid for temperature characterization, placed at the geometric center of the 1000 mm long tube furnace, open at both ends. A new, broadband two-color ratio pyrometry (TCRP) technique was developed independently in the laboratory and used for temperature characterization, with a cheap, commercial DSLR camera used as the pyrometer. This is the very first time that solid state temperature characterization has been performed in tube furnaces. Following are the major conclusions:

(1) The tube furnace was set to temperatures between 1000 K and 1426 K. After attainment of steady state, a total of 50 continuous images were acquired for intensity averaging and temperature measurement. TCRP yielded a temperature of 979.5 K ± 24% for a furnace temperature of 1000 K and a value of 1391 K ± 6.7% for a furnace wall temperature of 1426 K.

(2) Emission spectroscopy performed in the VIS-NIR (650 nm-1100 nm) gave temperatures within 4.5% of that from TCRP up to 1150 K, but the difference shot to a higher magnitude and reached as high as 8.6% for 1426 K, where it gave a metal temperature of 1290 K as opposed to TCRP's 1391 K. Although the most accurate technique in principle, this discrepancy may be attributed to experimental errors in emission spectroscopy. Analytical heat balance performed on the metal sheet, gave temperatures very close to that from TCRP, within ±2.5% to be precise. Numerical simulations performed in Ansys Fluent yielded temperature values within 5% of that of TCRP, thereby validating the accuracy of TCRP. As a final check of the accuracy of TCRP, a calibrated IR thermal imaging camera was aimed at several locations on the heated SS sheet and the mean temperature was noted. The IR camera yielded a temperature of 940 K, 1340 K and 1353 K for a furnace wall temperature of 1000 K, 1400 K and 1426 K respectively. These values are within 4% of that of TCRP. The comparisons increase confidence in the accuracy of TCRP.

(3) This work shows the high precision and appropriateness of TCRP for temperature characterization in tube furnaces. It can very easily be extended to ceramics or other class of solid materials that can be shown to behave as gray bodies in the visible region through measurements.

Acknowledgements

Technical discussions with Dr Yedhu Krishna, a colleague in the laboratory, have been of immense help to the first author. This work was funded by the Defence Research and Development Organization, India (grant number 0626).

References

[1]G. Che, B. B. Lakshmi, C. R. Martin, E. R. Fisher, and R. S. Ruoff, "Chemical vapor deposition based synthesis of carbon nanotubes and nanofibers using a template method," Chemistry of Materials **10**(1), 260-267 (1998).
[2]J. Q. Hu, X. L. Ma, N. G. Shang, Z. Y. Xie, N. B. Wong, C. S. Lee, and S. T. Lee, "Large-scale rapid oxidation synthesis of SnO2 nanoribbons," The Journal of Physical Chemistry B **106**(15), 3823-3826 (2002).
[3]Q. Wu, Z. Hu, X. Wang, Y. Lu, X. Chen, H. Xu, and Y. Chen, "Synthesis and characterization of faceted hexagonal aluminum nitride nanotubes," Journal of the American Chemical Society **125**(34), 10176-10177 (2003).
[4]H. Liu, Y. Li, S. Xiao, H. Gan, T. Jiu, H. Li, L. Jiang, D. Zhu, D. Yu, B. Xiang, and Y. Chen, "Synthesis of organic one-dimensional nanomaterials by solid-phase reaction," Journal of the American Chemical Society **125**(36), 10794-10795 (2003).
[5]J. Holcombe, and S. R. Koirtyohann, "The Downingtown furnace atomic absorption workshop: a report," Spectrochimica Acta Part B: Atomic Spectroscopy **39**(2-3), 243-248 (1984).
[6]M. Sperling, B. Welz, J. Hertzberg, C. Rieck, and G. Marowsky, "Temporal and spatial temperature distributions in transversely heated graphite tube atomizers and their analytical characteristics for atomic absorption spectrometry," Spectrochimica Acta Part B: Atomic Spectroscopy **51**(9-10), 897-930 (1996).
[7]B. Welz, M. Sperling, G. Schlemmer, N. Wenzel, and G. Marowsky, "Spatially and temporally resolved gas phase temperature measurements in a Massmann-type graphite tube furnace using coherent anti-Stokes Raman scattering," Spectrochimica Acta Part B: Atomic Spectroscopy **43**(9-11), 1187-1207 (1988).
[8]W. Frech, and D. C. Baxter, "Temperature dependence of atomization efficiencies in graphite furnaces," Spectrochimica Acta Part B: Atomic Spectroscopy **45**(8), 867-886 (1990).
[9]B. V. L'vov, D. A. Katskov, L. P. Kruglikova, and L. K. Polzik, "Absolute analysis by flame atomic absorption spectroscopy: present status and some problems," Spectrochimica Acta Part B: Atomic Spectroscopy **31**(2), 49-80 (1976).
[10]A. Purwar, and S. Deep, "A novel thermocouple for ultra high temperature applications: Design and computational analysis," in *Consumer Electronics-Asia (ICCE-Asia)* (IEEE, 2017), pp. 145-150.
[11]T. Mitani, M. Takahashi, S. Tomioka, T. Hiraiwa, and K. Tani, "Analyses and application of gas sampling to scramjet engine testing," Journal of Propulsion and Power **15**(4), 572-577 (1999).
[12]C. S. Park, M. E. Newfield, D. G. Fletcher, and T. Gokcen, "Spectroscopic measurements of shock-layer flows in an arcjet facility," Journal of thermophysics and heat transfer **13**(1), 60-67 (1999).
[13]M. P. Lee, B. K. McMillin, and R. K. Hanson, "Temperature measurements in gases by use of planar laser-induced fluorescence imaging of NO," Applied Optics **32**(27), 5379-5396 (1993).
[14]C. Gerardi, J. Buongiorno, L. W. Hu, and T. McKrell, "Study of bubble growth in water pool boiling through synchronized, infrared thermometry and high-speed video," International Journal of Heat and Mass Transfer **53**(19-20), 4185-4192 (2010).
[15]C. L. Chakrabarti, S. Wu, R. Karwowska, J. T. Rogers, L. Haley, P. C. Bertels, and R. Dick, "Temperature of platform, furnace wall and vapour in a pulse-heated electrothermal graphite furnace in atomic absorption spectrometry," Spectrochimica Acta Part B: Atomic Spectroscopy **39**(2-3), 415-448 (1984).
[16]W. M. Tolles, J. W. Nibler, J. R. McDonald, and A. B. Harvey, "A review of the theory and application of coherent anti-Stokes Raman spectroscopy (CARS)," Applied Spectroscopy **31**(4), 253-271 (1977).
[17]Y. A. Levendis, K. R. Estrada, and H. C. Hottel, "Development of multicolor pyrometers to monitor the transient response of burning carbonaceous particles," Review of scientific instruments **63**(7), 3608-3622 (1992).
[18]V. C. Raj, and S. V. Prabhu, "Measurement of surface temperature and emissivity of different materials by two-colour pyrometry," Review of Scientific Instruments **84**(12), 124903 (2013).
[19]W. Lee, and Y. D. Na, "Soot study in laminar diffusion flames at elevated pressure using two-color pyrometry and Abel inversion," JSME International Journal Series B Fluids and Thermal Engineering **43**(4), 550-555 (2000).
[20]F. Wang, X. J. Wang, Z. Y. Ma, J. H. Yan, Y. Chi, C. Y. Wei, M. J. Ni, and K. F. Cen, "The research on the estimation for the NOx emissive concentration of the pulverized coal boiler by the flame image processing technique," Fuel **81**(16), 2113-2120 (2002).
[21]F. Zander, "Surface temperature measurements in hypersonic testing using digital single-lens reflex cameras," Journal of Thermophysics and Heat Transfer **30**(4), 919-925 (2016).
[22]J. M. Densmore, B. E. Homan, M. M. Biss, and K. L. McNesby, "High-speed two-camera imaging pyrometer for mapping fireball temperatures," Applied optics **50**(33), 6267-6271 (2011).
[23]S. Srinath, and K. P. J. Reddy, "Large carbon cluster thin film gauges for measuring aerodynamic heat transfer rates in hypersonic shock tunnels," Measurement Science and Technology **26**(2), 025901 (2015).

[24]D. Ng, and G. Fralick, "Use of a multiwavelength pyrometer in several elevated temperature aerospace applications," Review of Scientific Instruments **72**(2), 1522-1530 (2001).
[25]R. Polini, B. Paci, A. Generosi, and G. Marcheselli, "Synthesis of scheelite nanoparticles by mechanically assisted solid-state reaction of wolframite and calcium carbonate," Minerals Engineering 138, 133-138 (2019).
[26]T. Fu, X. Cheng, C. Shi, M. Zhong, T. Liu, and X. Zheng, "The set-up of a vision pyrometer," Measurement Science and Technology **17**(4), 659 (2006).
[27]S. Deep, and G. Jagadeesh, "Aerothermodynamic effects of controlled heat release within the hypersonic shock layer around a large angle blunt cone," Physics of Fluids **30**(10), 106103 (2018).
[28]B. K. Gunturk, J. Glotzbach, Y. Altunbasak, R. W. Schafer, and R. M. Mersereau, "Demosaicking: color filter array interpolation," IEEE Signal processing magazine **22**(1), 44-54 (2005).
[29]T. L. Bergman, F. P. Incropera, D. P. DeWitt, and A. S. Lavine, *Fundamentals of heat and mass transfer* (John Wiley & Sons, 2011).
[30]J. Canny, "A computational approach to edge detection," in *IEEE Transactions on Pattern Analysis and Machine Intelligence 6* (IEEE, 1986), pp. 679–698.
[31]A. N. Magunov, "Spectral pyrometry," Instruments and experimental techniques **52**(4), 451-472 (2009).
[32]R. J. Moffat, "Describing the uncertainties in experimental results," Experimental thermal and fluid science **1**(1), 3–17 (1988).

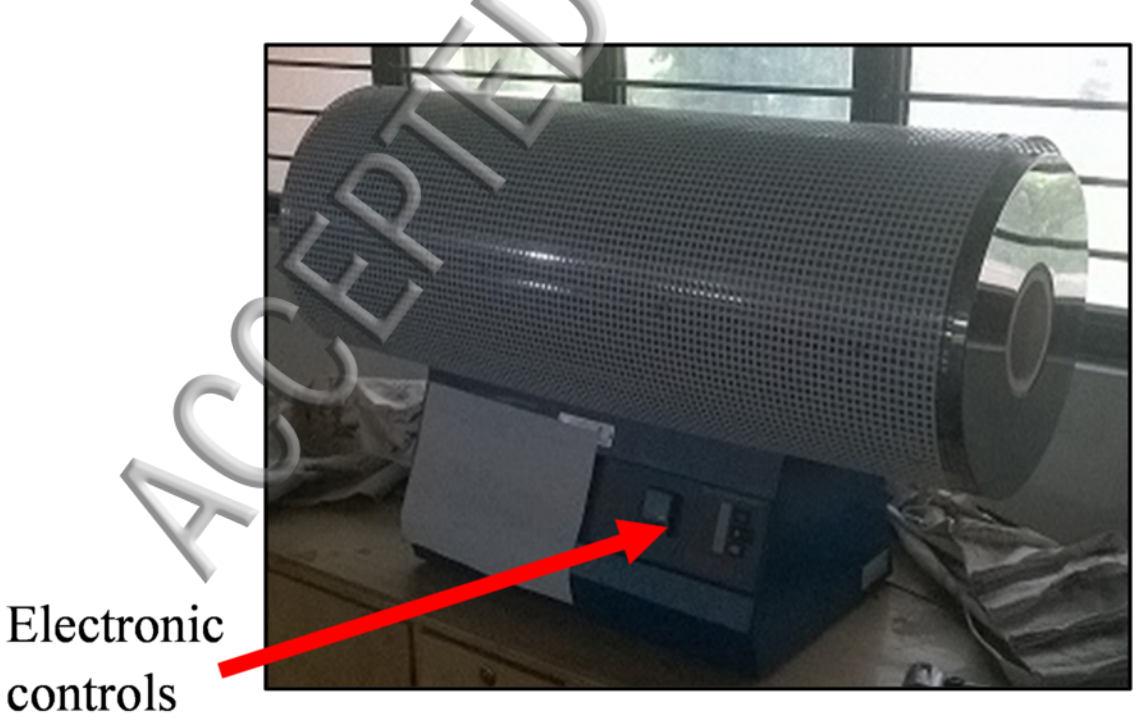
Electronic
controls

(a)


Sillimanite working tube
Heating wire element

(b)

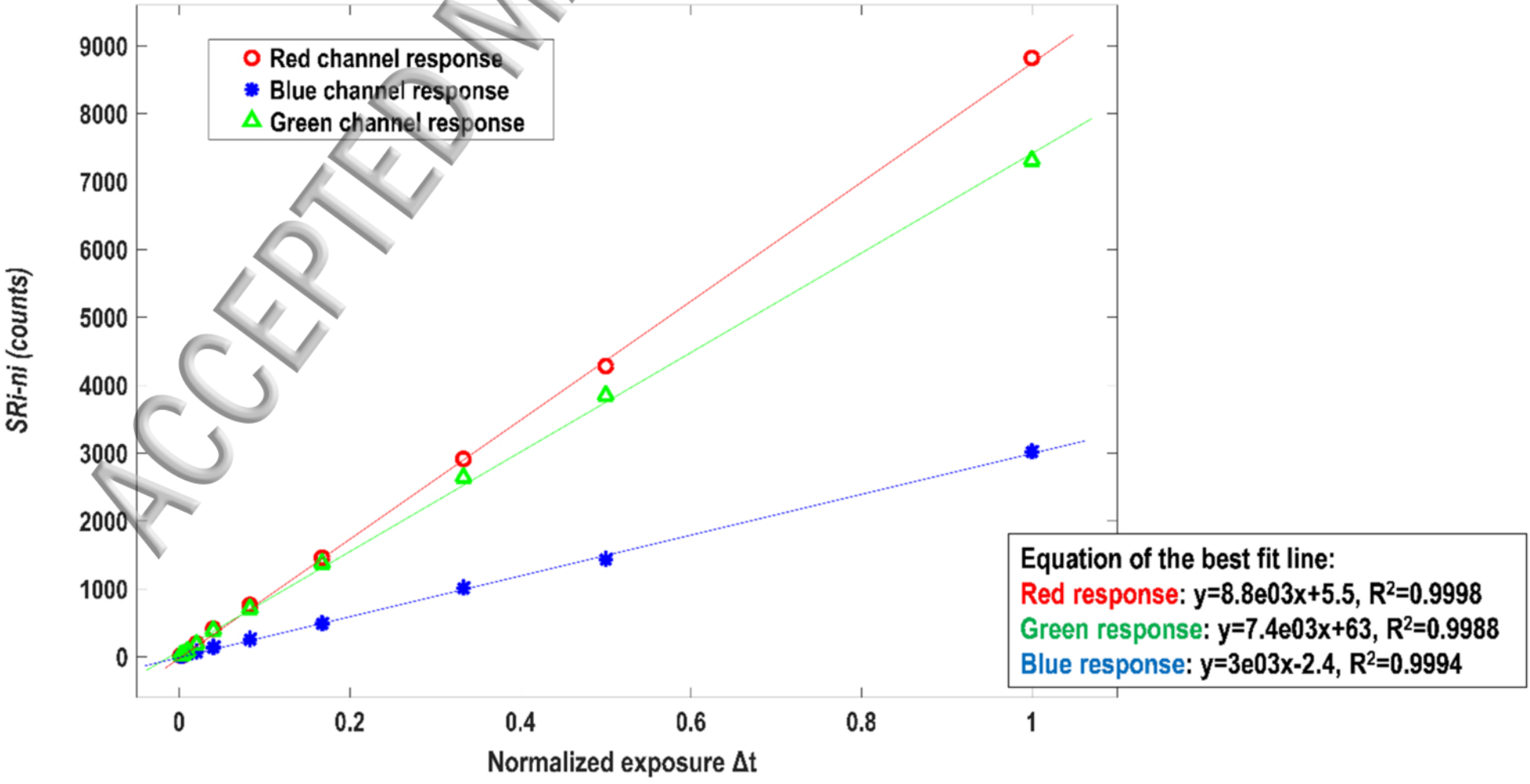
Red channel response
Blue channel response
Green channel response
SRi-ni (counts)
Normalized exposure Δt
0
1000
2000
3000
4000
5000
6000
7000
8000
9000
0
0.2
0.4
0.6
0.8
1
Equation of the best fit line:
Red response: y=8.8e03x+5.5, R²=0.9998
Green response: y=7.4e03x+63, R²=0.9988
Blue response: y=3e03x-2.4, R²=0.9994

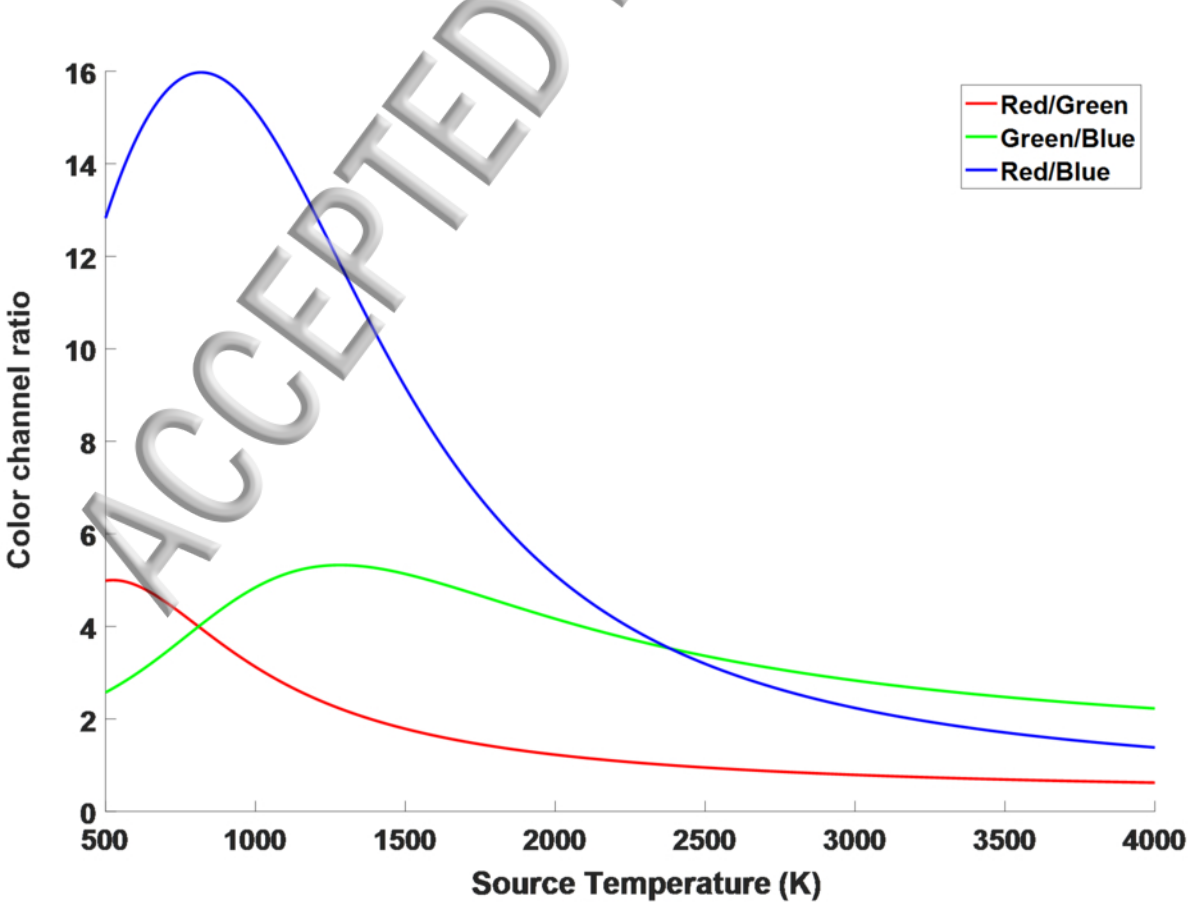
Red/Green
Green/Blue
Red/Blue
Color channel ratio
Source Temperature (K)
0
2
4
6
8
10
12
14
16
500
1000
1500
2000
2500
3000
3500
4000

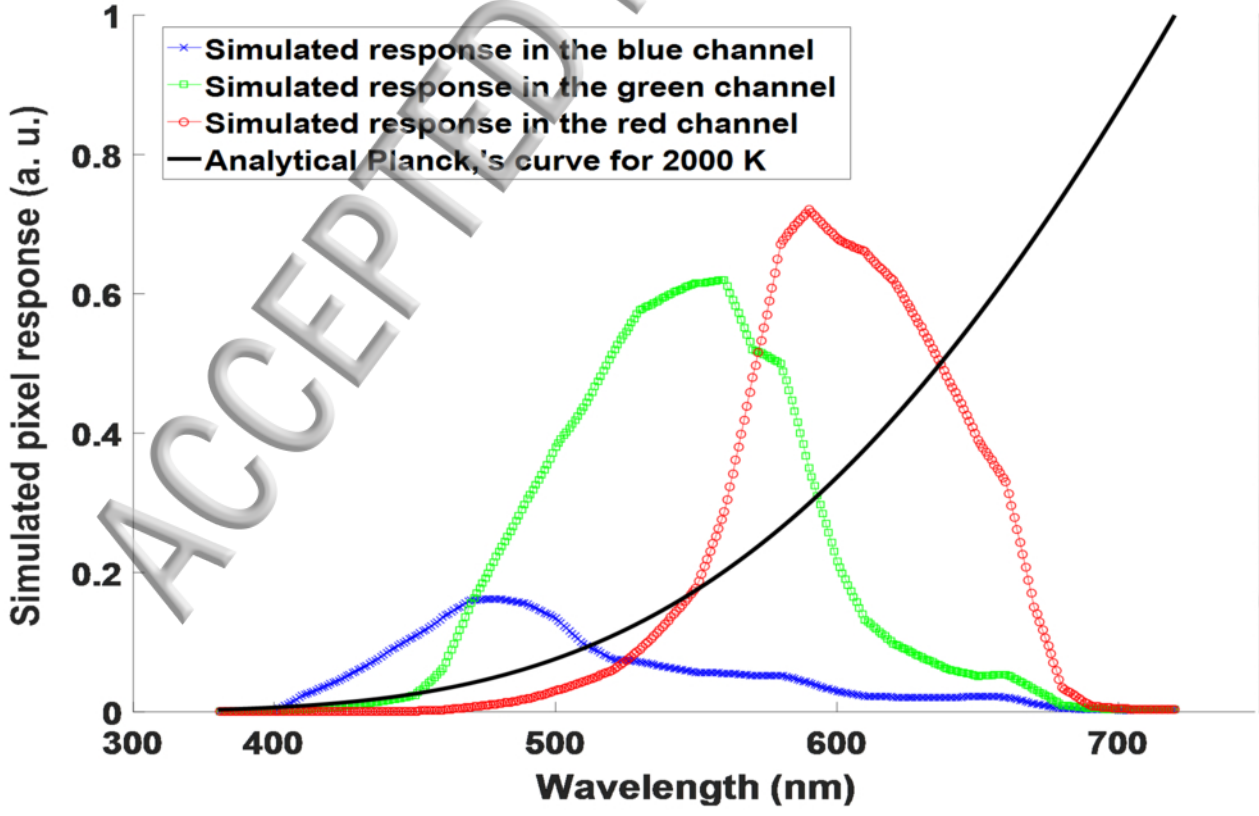

(a)

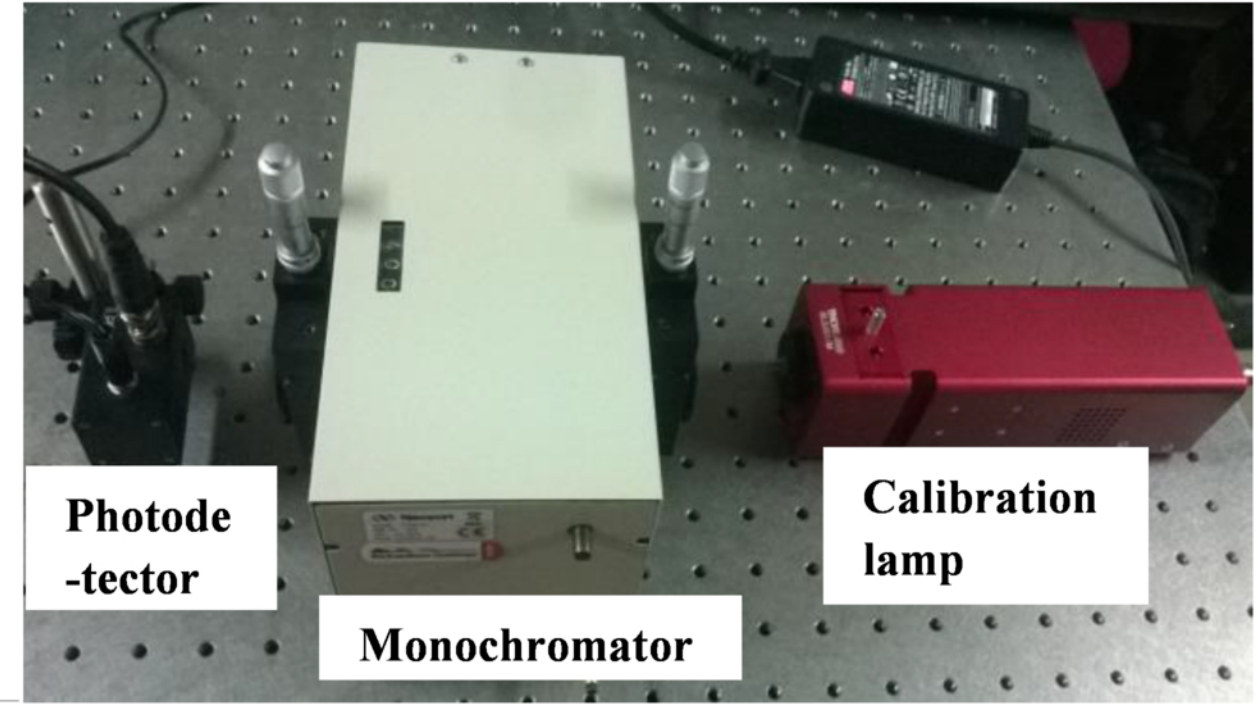

(b)

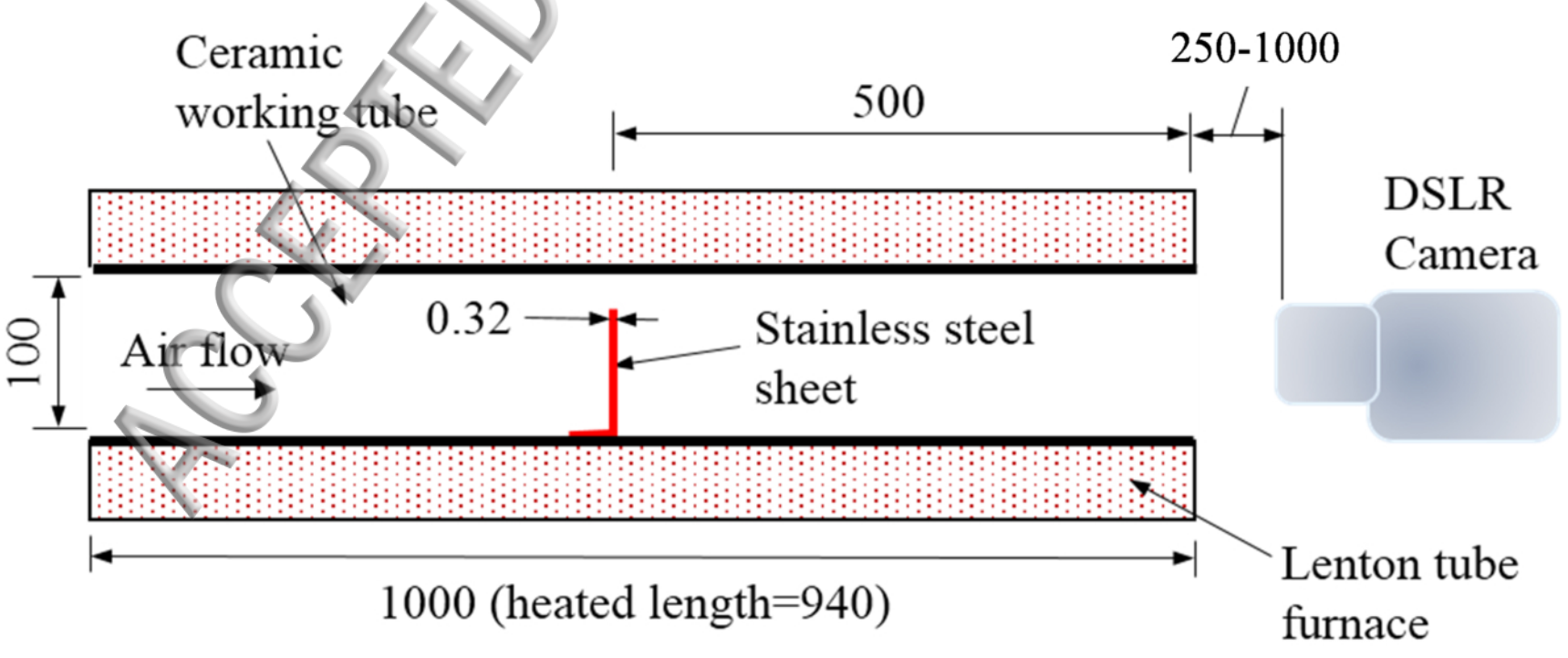

SIDE VIEW

All dimensions are in mm.

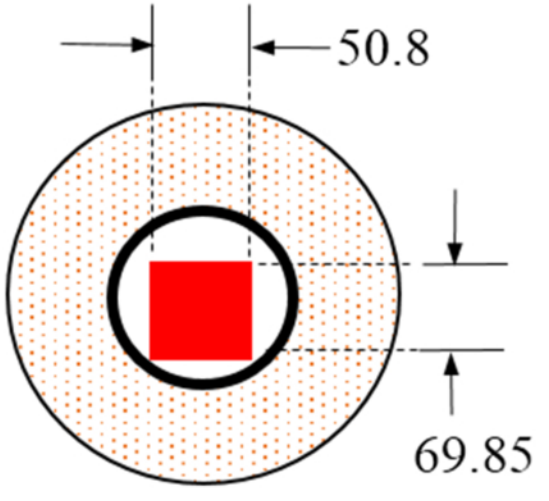

FRONT VIEW

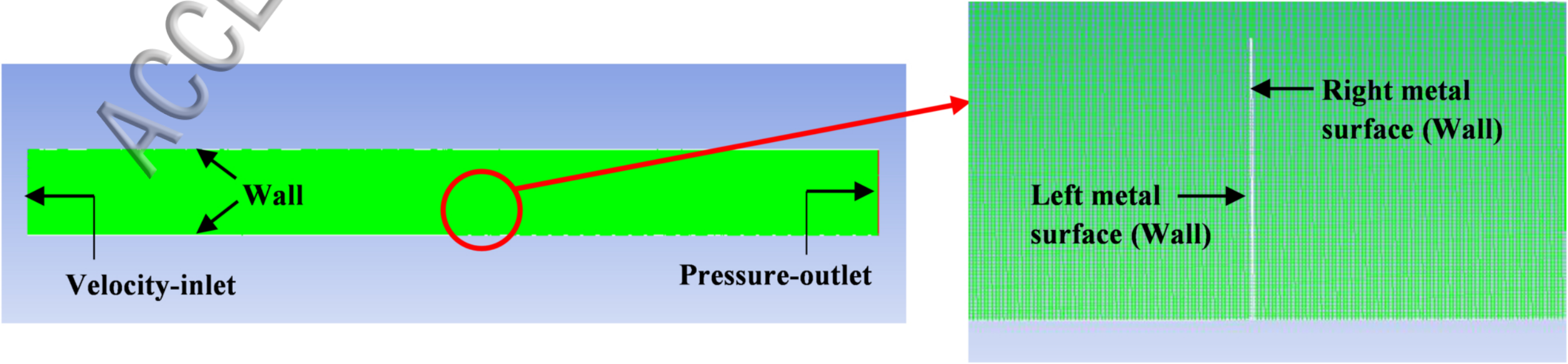
Wall
Velocity-inlet
Pressure-outlet
Right metal surface (Wall)
Left metal surface (Wall)

1000 K, Exposure:4 sec

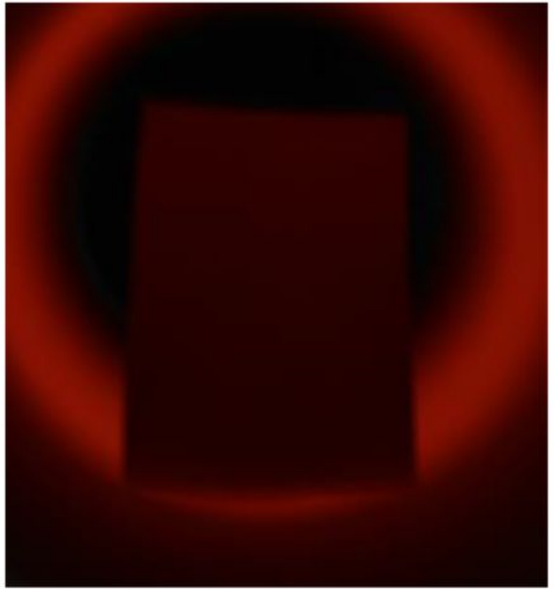

1100 K, Exposure:1/2 sec

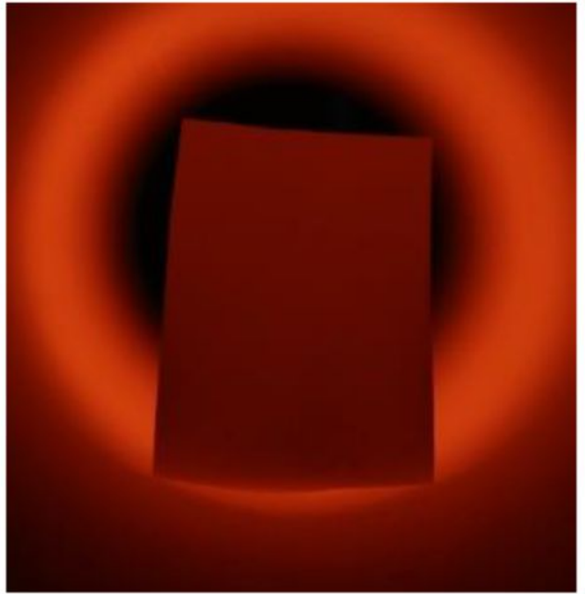

1250 K, Exposure:1/10 sec

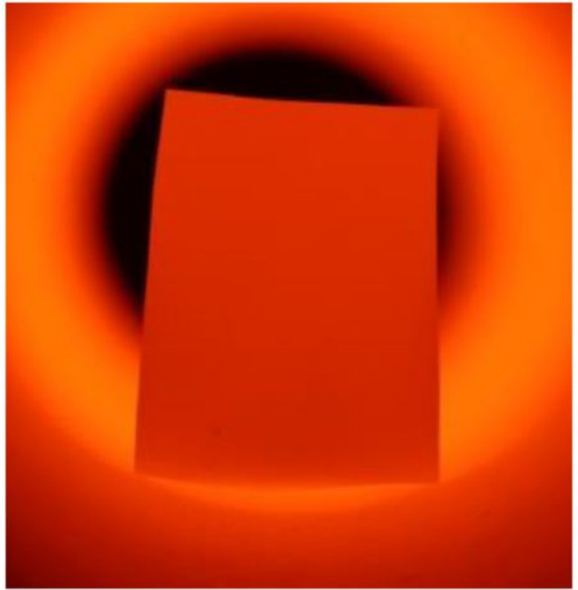

1426 K, Exposure:1/50 sec

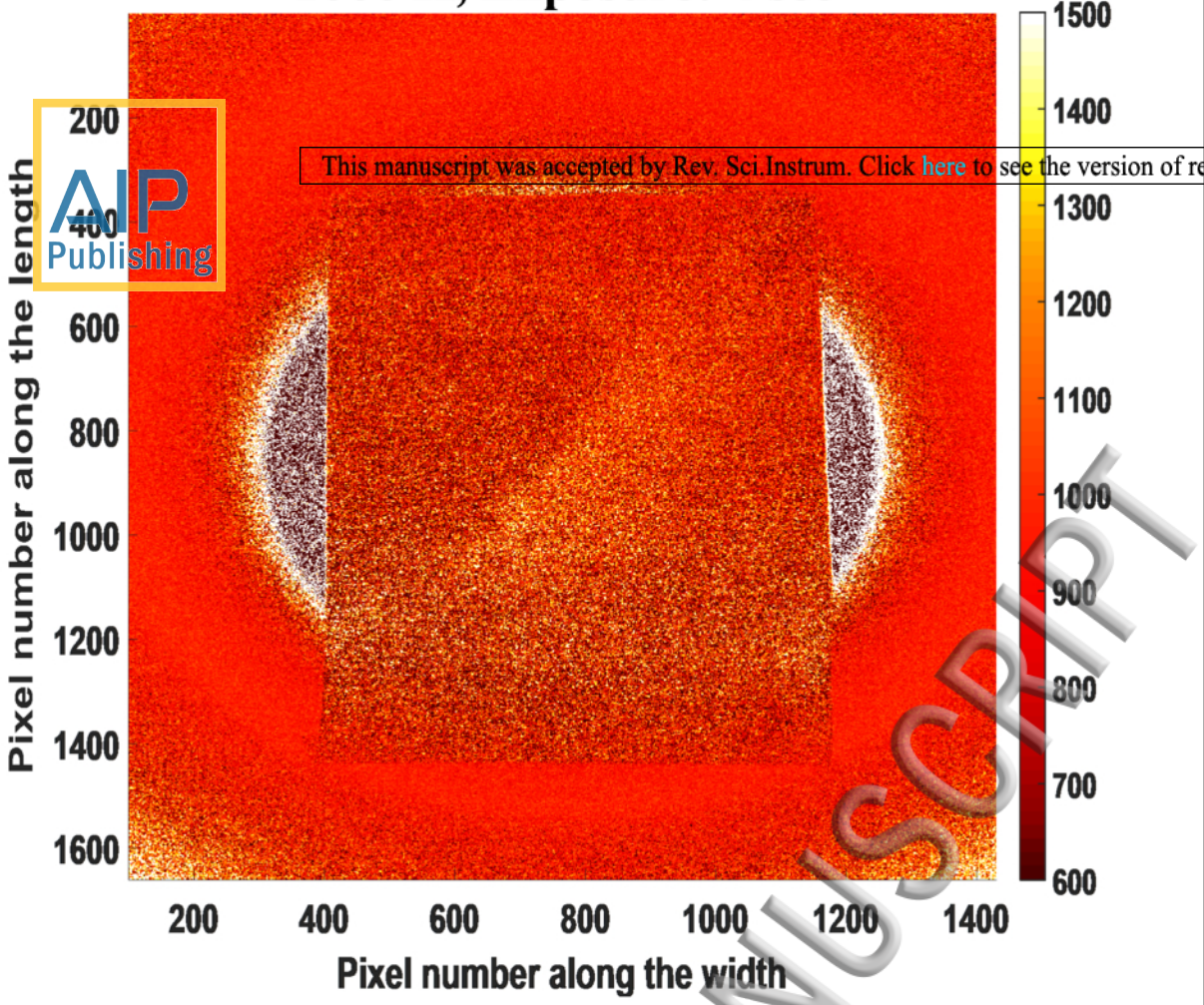

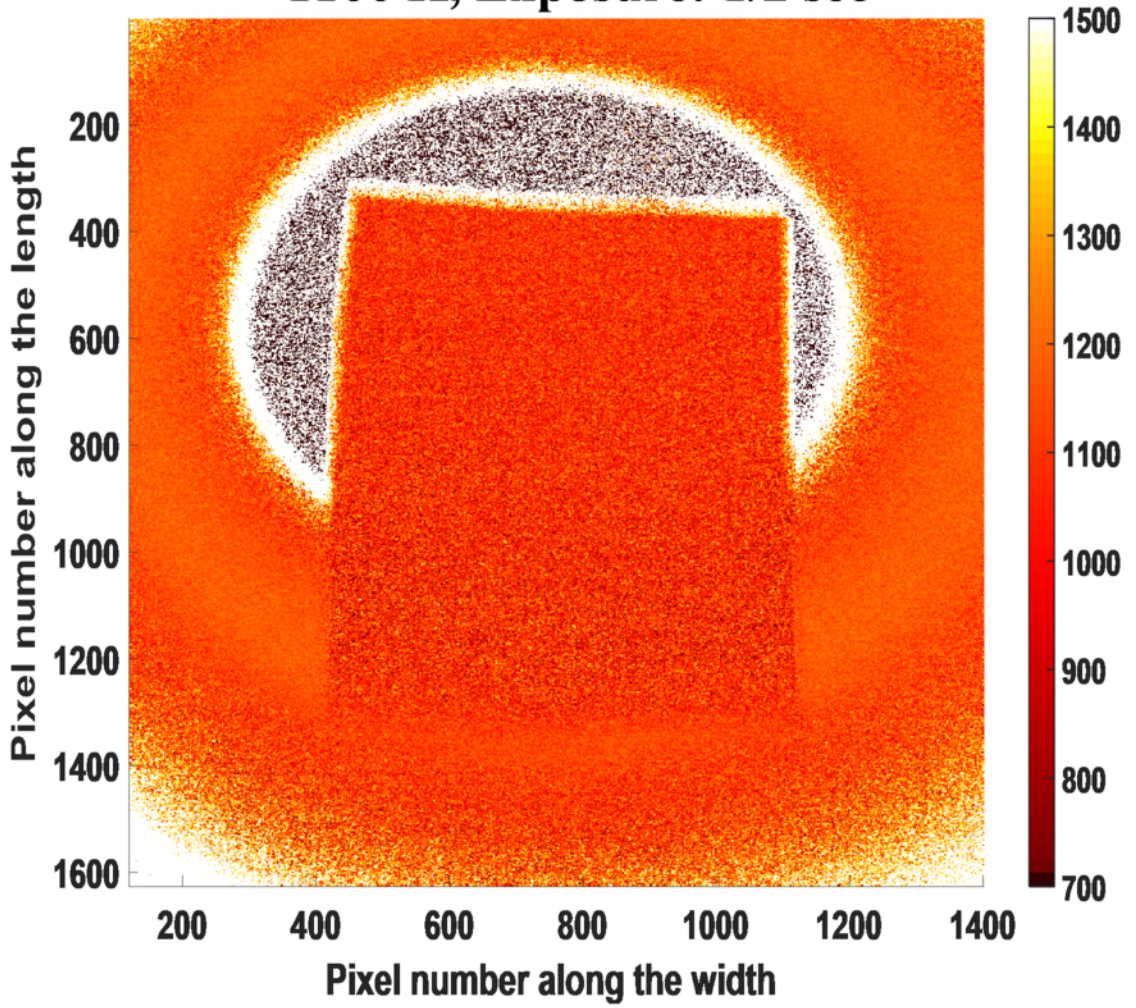

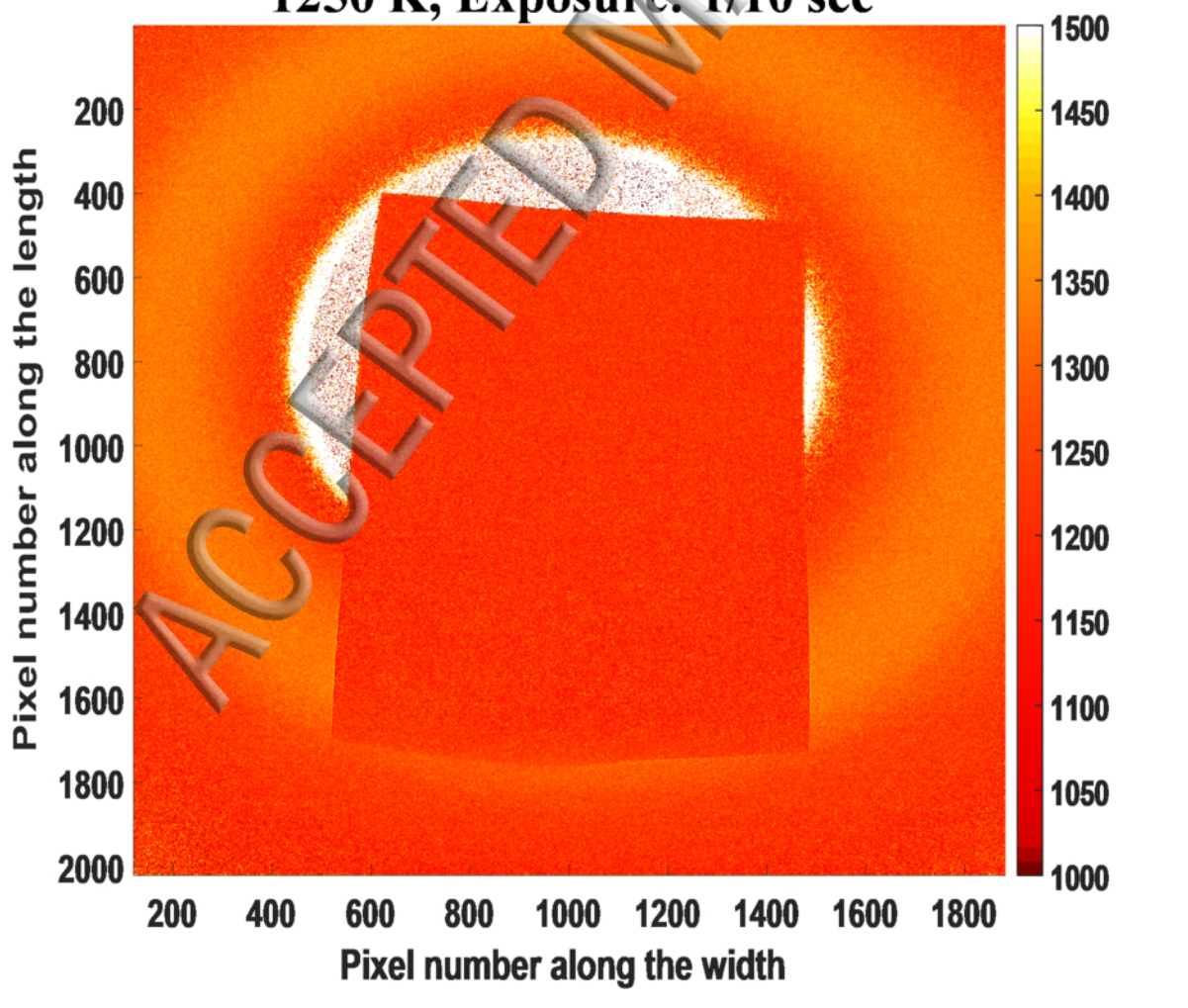

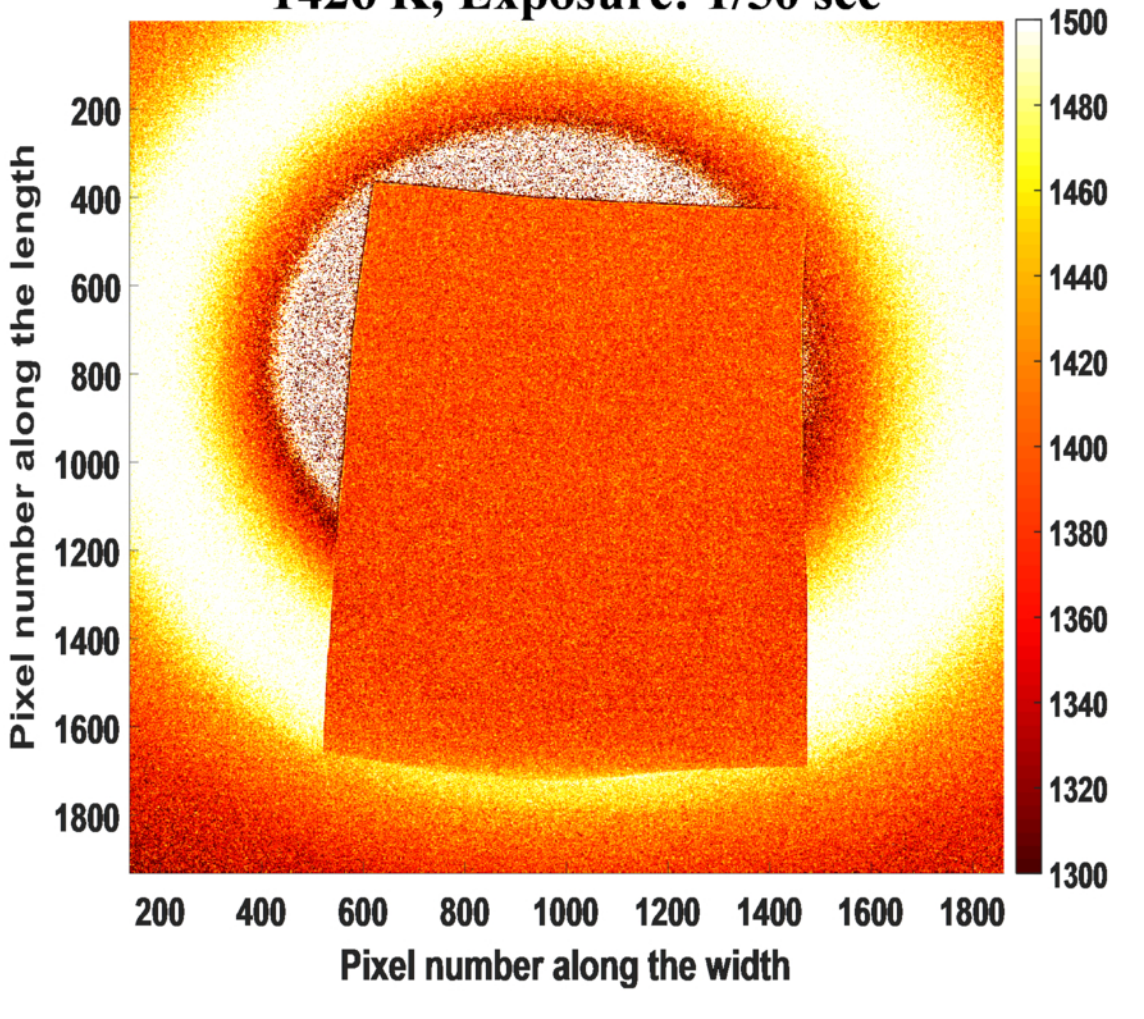

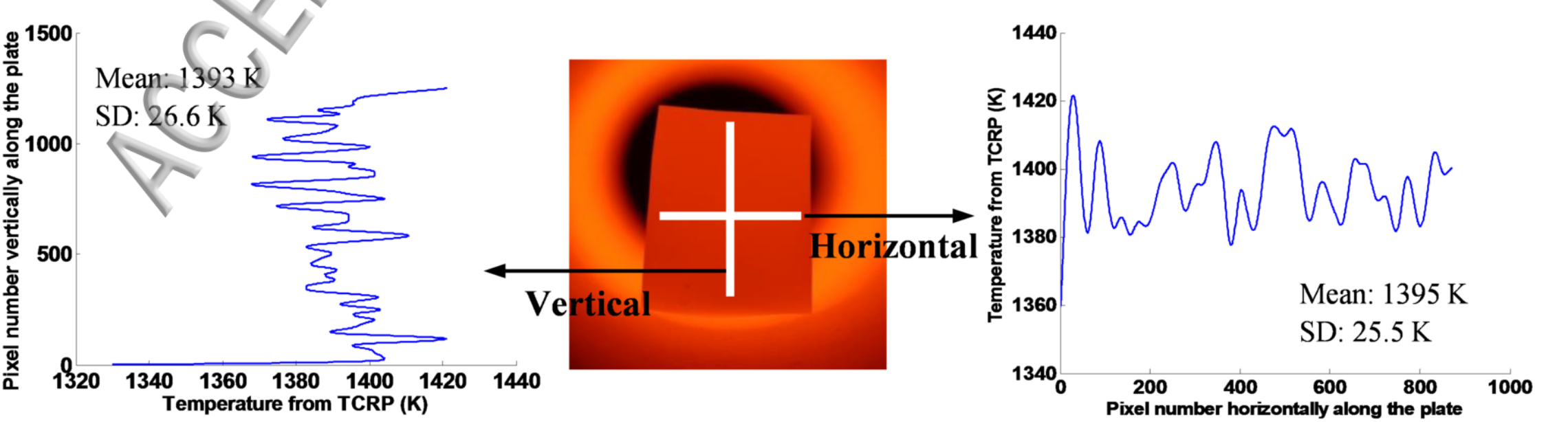
Mean: 1393 K
SD: 26.6 K
Pixel number vertically along the plate
Temperature from TCRP (K)
Vertical
Horizontal
Temperature from TCRP (K)
Mean: 1395 K
SD: 25.5 K
Pixel number horizontally along the plate

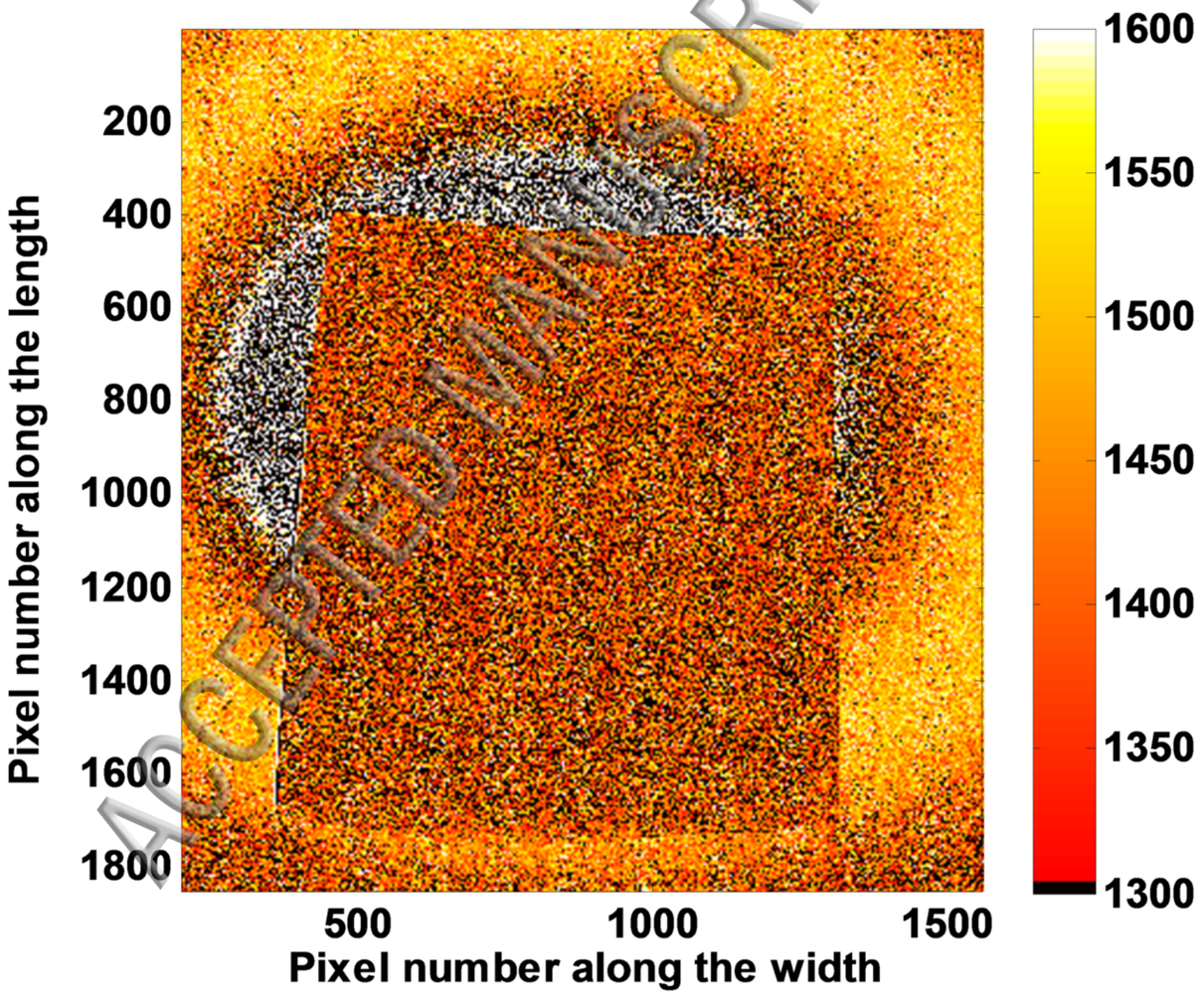

(a)

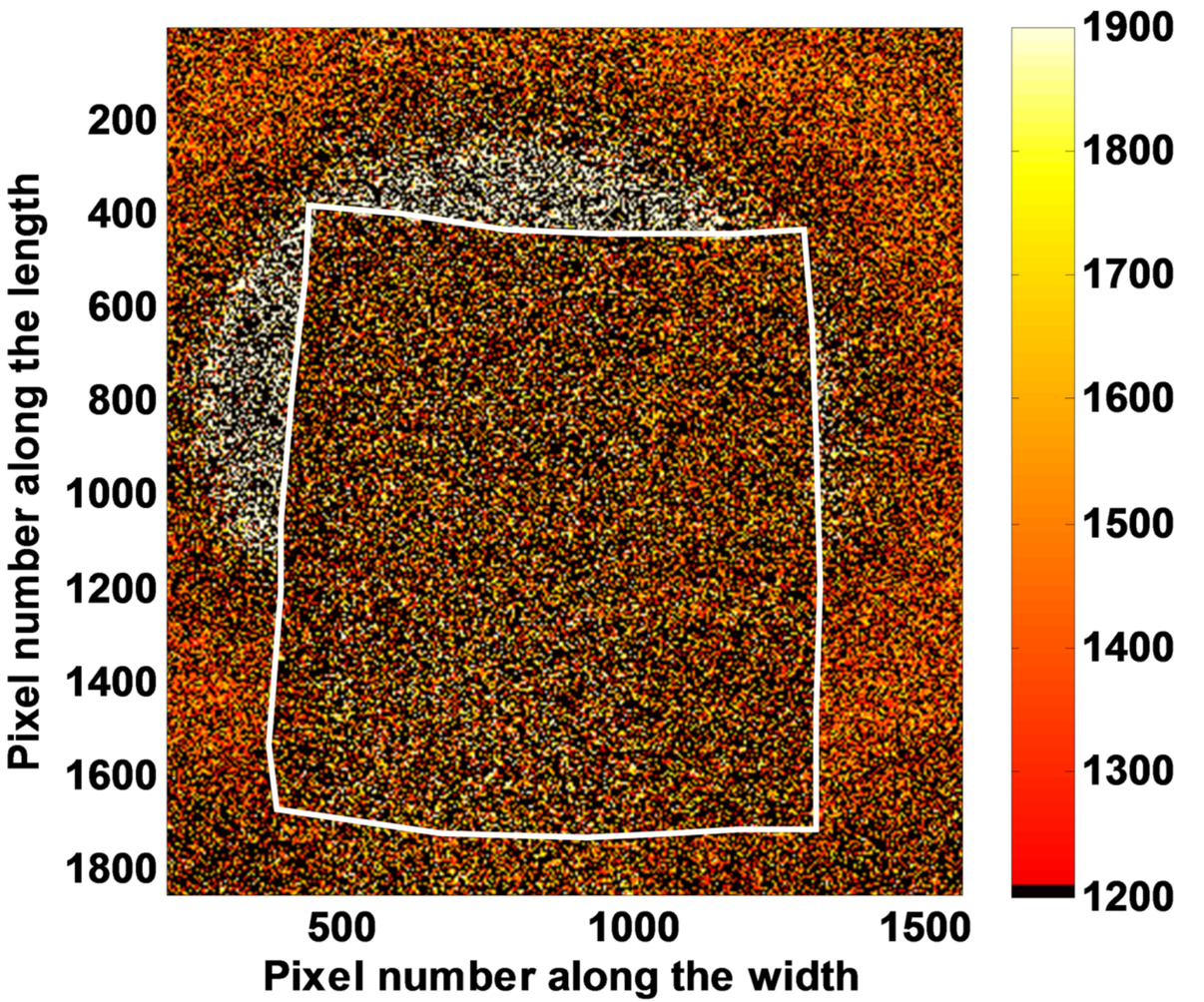

(b)

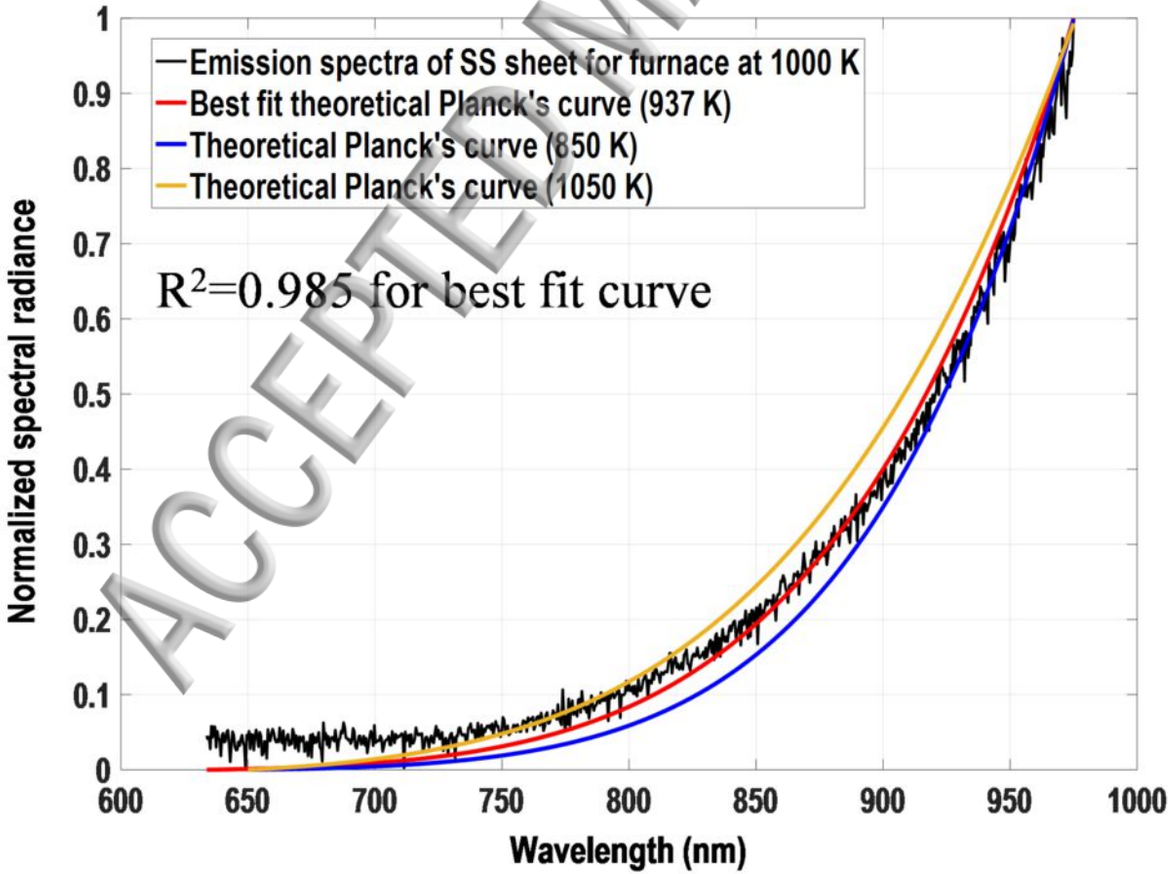

(a)

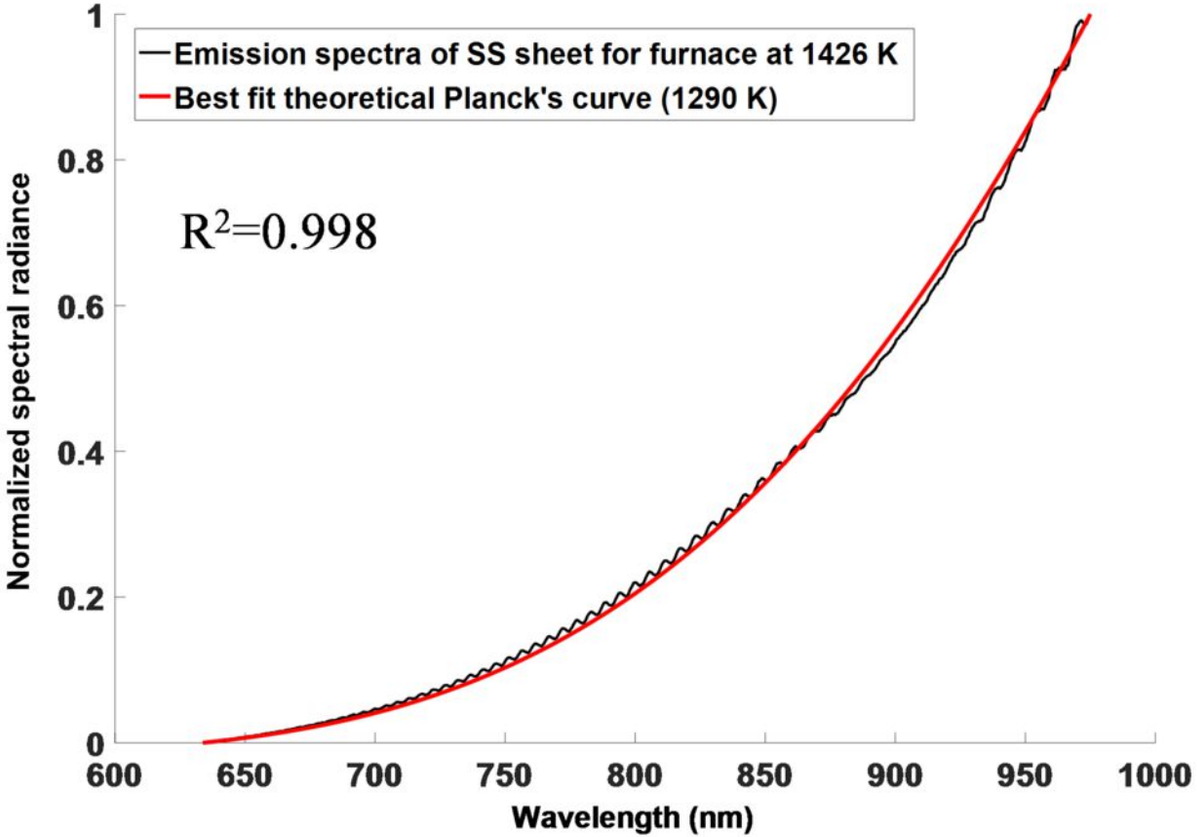

(b)

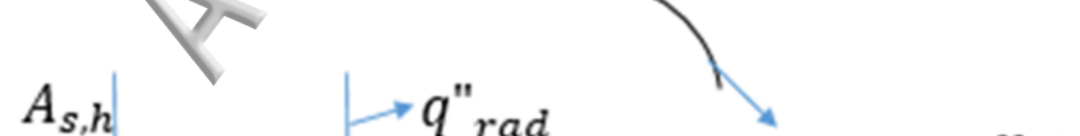

$$T_{t=0} = T_i = 300\ K$$

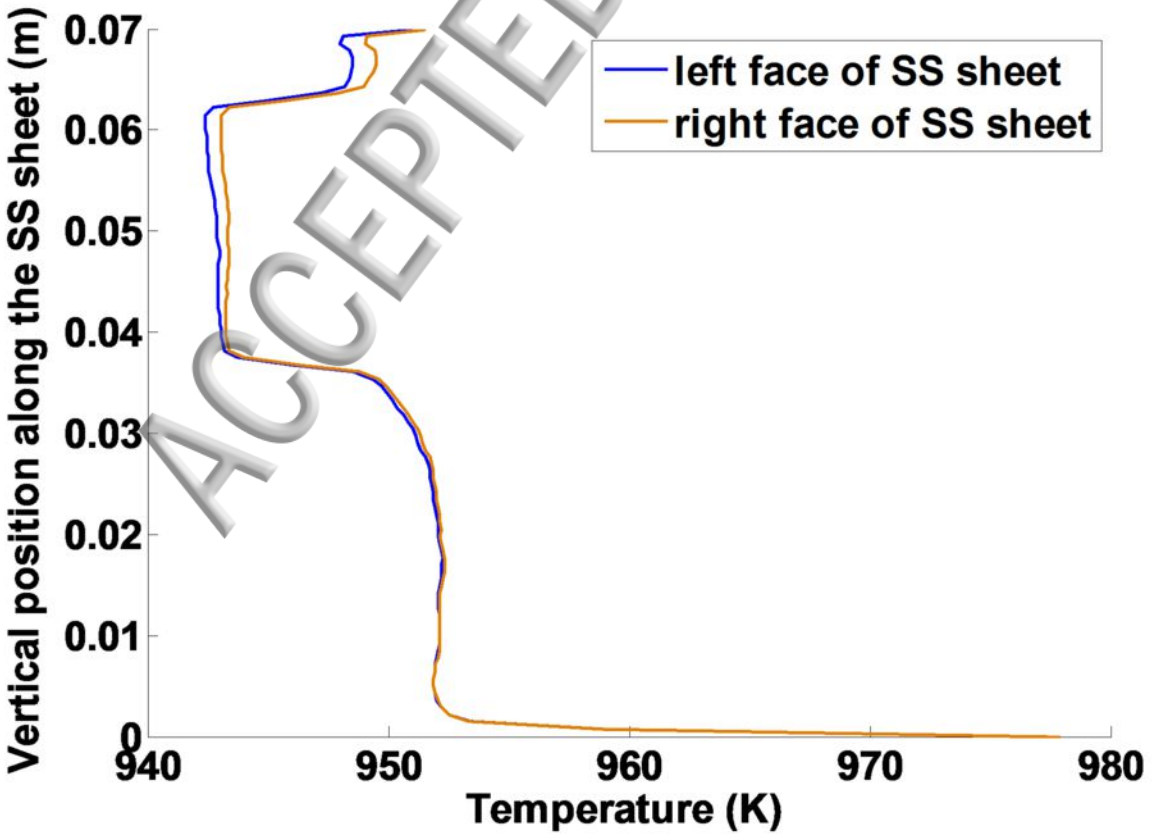
left face of SS sheet
right face of SS sheet
Vertical position along the SS sheet (m)
0.07
0.06
0.05
0.04
0.03
0.02
0.01
0
940
950
960
970
980
Temperature (K)

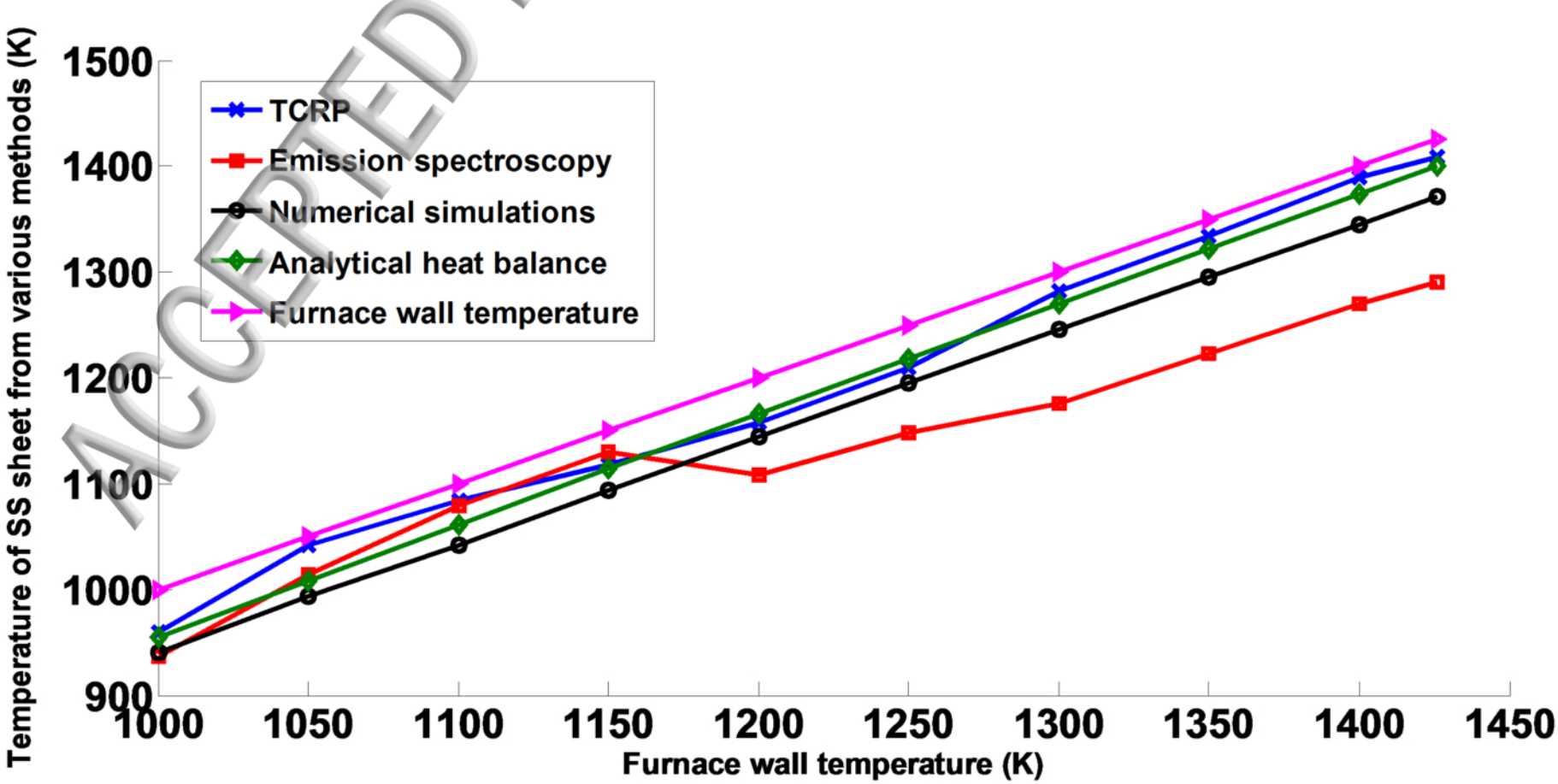
TCRP
Emission spectroscopy
Numerical simulations
Analytical heat balance
Furnace wall temperature
Temperature of SS sheet from various methods (K)
Furnace wall temperature (K)
1500
1400
1300
1200
1100
1000
900
1000
1050
1100
1150
1200
1250
1300
1350
1400
1450